博士論文

Application of TOT and BPCA methods to the reconstruction of past biomass burning from sediment archives

(熱光透過法およびベンゼンポリカルボン酸法を応用した堆積物記録からの過去のバイオマス燃焼復元)

北海道大学　大学院環境科学院
地球圏科学専攻
芦　松　　(Lu Song)

Contents

List of illustrations

List of Table

Abstract

Behavior of black carbon (BC) is crucial for the earth's surface environment because it could cause global warming by absorbing sunlight in the atmosphere. BC is originated from incomplete combustion of biomass or fossil fuels. Combustion in natural processes is incomplete due to local limitation of oxygen during the fire, which leads to the formation of organic fire residues. Robustness of BC to degradation in the natural environment (in soils or sediment) enables us to use BC as a proxy to study the frequency and burning temperatures of past wildfire events. But the previous paleofire researches only measured charcoals in sediments and discussed the local biomass burning history in spite of the significance of fine BC for atmospheric radiation budget. Controlling factors for burning temperature also has not been evaluated well.

Objective of this study is to understand factors controlling the thermal/optical/chemical/size characters of BC in relation to the variabilities of burning temperature, provenance and aging as well as the vegetation in the hinterland. For these purposes, BC was quantified as elemental carbon (EC) in coarse (>2 μm) and fine (<2 μm) fractions of sediment samples using a thermal optical transmittance (TOT) method, and their burning temperatures were estimated for bulk samples through measurement of composition of benzene polycarboxylic acids (BPCAs), molecular markers of fire residues, determined with high performance liquid chromatography (HPLC).

Selected plants were experimentally charred to obtain standard charcoal samples, which were served as model BC materials to calibrate BPCA compositions to the pyrolysis treatment temperature. The TOT and BPCA methods were applied to marine and lake sediments such as the surface sediments collected during KR15-10 cruise off the Wakasa Bay, 63 samples between 0 and 203 m core composite depth (CCSF-D) selected from IODP Site U1423 in the northeastern Japan Sea which covered the last 4.3 Myr, and 15 samples selected from SG12 at the Lake Suigetsu which covered the last 15 kyr. Size dependencies of EC contents and thermal properties were compared with the contents and composition of BPCAs to examine the influences of sources, transport pathways, and burning temperatures of BCs contained in these sediment archives. The TOT and BPCA methods were also applied to the sediments samples to trace the changes of BC upon aging in sediments.

The author also compared the thermal characteristics of BC determined by TOT method and BPCA compositions in order to verify the methods determining the amount and composition of BC in sediment archives. It could be shown that TOT and BPCA were valuable tool to determine BC in sediments samples due to its resistivity to (bio-)chemical degradation even for the past million years, and allow us to estimate the burning temperature of BC in sediments.

Chapter 1. Introduction

1.1. Environmental significance of black carbon

Fire has played an important role in the evolution of plants and terrestrial ecosystems and has the history as long as that of land plants (Bowman et al., 2009; Bowman et al., 2011). Black Carbon (BC) is the main solid product of fires, they are widely derived from biomass burning and fossil fuel combustion, such as agriculture, forest fires, and industrial production (Thevenon et al., 2010; Scott, 2010; Daniau et al., 2012; Chakrabarty et al., 2015). The color of BC allows them to absorb radiant energy (Bond and Bergstrom, 2006; Bond et al., 2013; Buseck et al., 2014; Khan, 2016) and potentially affects the climate (Oshima et al., 2012; Hodnebrog et al., 2016). BC and minerals are combined to form stable particles (Lützow et al., 2006; Guggenberger et al., 2008), so that BC can be stored for long periods in environments (Swift, 2001; Masiello et al., 2002; Masiello, 2004; Czimczik and Masiello, 2007).

Regional biomass burning of general frequency is related to the volume of vegetation, frequency of ignition events, and connectivity of the fuel bed (Archibald et al., 2012; Lehmann et al., 2014), where these factors could be controlled by climate change (Thevenon et al., 2010; Marlon et al., 2013; Lu et al., 2018; Lu et al., 2019). Although these seems to be little human influence on fire regimes before the Holocene (Marlon et al., 2008; Daniau et al., 2012 Marlon et al., 2012; Marlon et al., 2013), but there is a

major contribution of humans to the ignition of present-day fires (Marlon et al., 2008; Thevenon et al., 2010; Archibald et al., 2012; Marlon et al., 2013). Much of what we have learned about the interactions between fire and climate, and the role of fire in shaping modern ecosystems is derived from sedimentary charcoal records (Bowman et al., 2009; Scott, 2000; Scott, 2010; Bowman et al., 2011). It is expensive and time consuming to analyze the BC content of deep sea sediments, so there has been little consideration of how fire regime behave on million years timescales and beyond the range of recent climates (Scott, 2000; Masiello, 2004; Bowman et al., 2009; Krawchuk et al., 2009; Zhang et al., 2015b; Zhang et al., 2015a). This is an issue that can be addressed using marine sedimentary micro charcoal or soot records.

1.2. Definition of Black Carbon (BC)

BC is a part of the continuously combustion continuum residue (Masiello et al., 2002; Masiello, 2004; Preston and Schmidt, 2006; Wolf et al., 2013) defined as "combustion produced black particulate carbon having a graphitic microstructure" (Novakov, 1984; Grosjean et al., 1994; Sato et al., 2003; Buseck et al., 2014), the range of structures is often described as a continuum from partially charred plant materials that still retain their physical structure, to charcoal, soot and ultimately graphite (Seiler and Crutzen, 1980; Gustafsson and Gschwend, 1998; Glaser and Amelung, 2003; Masiello, 2004; Preston and Schmidt, 2006) (Fig. 1).

1.3. BC transportation from fire center to sediment

As a kind of sediment, the diameter of the BC particles may reveal the information of the fire source or the transport history of the particles. Variation in process of BC deposition explained by the size of potential charcoal source areas (PCSAs) (Peters and Higuera, 2007; Black et al., 2014; Santín et al., 2016), generally speaking, human activities, biological disturbances, atmospheric factors and mechanical constraints will control BC deposition (Théry-Parisot et al., 2010). Previous studies have shown that micro charcoal comes from a wider area, while macro charcoal comes from local fire (Peters and Higuera, 2007; Black et al., 2014; Vachula et al., 2018a; Vachula et al., 2018b). The range of transport of macroscopic BC is limited, although coarse particles of EC may be transported out of a fire site by water (Scott, 2000), or by the river's secondary erosion (Théry-Parisot et al., 2010). Because, soils act as intermediate stage for the aging of BC prior to deposition in the ocean (Schmidt et al., 2002). Most of the BCs with a diameter of 100 ~ 10000 μm can only move from 0 to 40 km from the center of the fire (Clark, 1988; Whitlock and Millspaugh, 1996; Clark et al., 1998; Ohlson and Tryterud, 2000; Enache and Cumming, 2006; Tinner et al., 2006; Higuera et al., 2007; Higuera et al., 2011; Kelly et al., 2013; Oris et al., 2014; Li et al., 2017; Vachula and Richter, 2018) (Fig. 2). Individual BCs with a diameter of 10 to 100 μm can move more than 60 km (MacDonald et al., 1991; Miller et al., 2017).

On the other hand, fine BC (< 10 μm)can be transported over long distances more than

1000 of km (Masiello, 2004). BC particles with diameters less than 2 microns can float for a long time in the atmosphere (Thevenon et al., 2010; Chakrabarty et al., 2015). The transport distance of BC determines the scale of the charcoal source area, but previous studies have probably underestimated the scope of potential charcoal source area (Lynch et al., 2002). The results of such studies often do not take into account the diameter of BC particles. There are very few data on BC concentration and particle sizes from marine sediment (Masiello, 2004). So we need to discuss the origin of BCs with different particle diameters.

1.4. Detection & Quantification of BC

Because the BC actually covers wide variety of materials from slightly charred biomass to graphitic BC, so the method of quantifying BC is not the same among previous studies. Thermal optical transmittance analyses (TOT) is mainly used to quantify the BC content in aerosol samples, but it has been used as analytical methods that could provide reasonable estimates of BC content in sediments (Masiello, 2004; Hammes et al., 2007; Buseck et al., 2014). Elemental carbon (EC) is operational term for the carbon fragments measured using TOT analyses. Referring to the previous research results, EC could be defined as the high-temperature component of the analyses, whereas OC was the low-temperature component of the analyses (Buseck et al., 2014).

The benzene polycarboxylic acids (BPCA) method is another potential quantitative

approach which could provide thermal characteristics of BC (Glaser et al., 1998; Brodowski et al., 2005; Guggenberger et al., 2008). This method was previously used to quantify the BC content in soil samples (Yarnes et al., 2011; Singh et al., 2014; Boot et al., 2015). The yield of mellitic acid (B6CA) is closely related to the pyrolysis temperature of BC (Schneider et al., 2010; Schneider et al., 2011; Schneider et al., 2013). The principle of this method is based on the conversion of the condensed structures into benzene carboxylic acids through oxidation treatment using 65% HNO_3 at 170 °C for 8 hours (Schneider, 2011), which subsequently can be separated and quantified by high performance liquid chromatography - diode array detector (HPLC-DAD) (Dittmar, 2008; Schneider et al., 2011; Yarnes et al., 2011).

1.5. Forest fire temperature

Most fire temperature can cover a very wide range, ranging from 80 °C to 950 °C (Sah et al., 2006; Cohen-Ofri et al., 2006; Fierro et al., 2007; Wolf et al., 2013; Wolf et al., 2014). However, based on the type of biomass fuel and the location of the fire, the main pyrolysis temperature are concentrated on 350 °C, 550 °C and 850 °C (Wolf et al., 2013), ordinary temperatures in biomass burning are approximately 500 ~ 600 °C, whereas canopy fires can be much hotter (> 800 °C), and root smoldering can be much lower (< 400 °C). Therefore, we selected this temperature sequence in this study to make BC. We quantify the difference of thermal properties of biomass materials of five different plants at consistent pyrolysis temperature sequence.

Although the physical properties of charcoal from different biomass sources are similar (Théry-Parisot et al., 2010), there are differences in thermal properties, which limits use of molecular thermometers (Schneider et al., 2013). However, an improper pre-treatment step may reduce the reproducibility of the analytical method (Brodowski et al., 2005; Kaal et al., 2008), which could impairs the thermal characteristic information provided by the BPCA method (Wiedemeier et al., 2015; Wiedemeier et al., 2016). Moreover, studies on BC from different plant sources are limited (Schneider et al., 2010; Schneider et al., 2011; Schneider et al., 2013; Bostick et al., 2018).

1.6. Objectives

In this study, the relationship between biomass burning and vegetation (climate) changes in East Asia on the different time-scales from longer than 1000 ky to shorter than 15 ky are examined using marine and lake sediments that are anticipated to receive biomass burning products from the east Asian region. The relationship between the quality and quantity of laboratory-generated chars and heat treatment temperature in five plants is examined using BPCA molecular markers by HPLC analysis. In order to solve the problems mentioned in the sections above, the following objectives are raised;

1). Evaluation of the consistency between TOT and BPCA methods for BC quantification

2). Confirmation of BPCA applicability as a molecular thermometer to various plants

collected in east Asia

3). Examination of the aging effect on old sediment archives (> 1 Million years)

4). Reconstruction of biomass burning magnitude, temperature, and fine BC emission in the east Asian region of the past.

Chapter 2. Sediment cores

2.1. Site U1423 of the Japan Sea

Integrated Ocean Drilling Program (IODP) Expedition (Exp.) 346 Site U1423 is located in the eastern part of the Japan Basin at 41°41.95'N, 139°4.98'E and was recovered from a 1785 m water depth (Igarashi et al., 2018) (Fig. 3). Site U1423 is situated on the middle of the slope at Oshima Island and is under the direct influence of the Tsushima Warm Current (TWC). The TWC flows toward the Tsugaru Strait and the Soya Strait (Yoon and Kawamura, 2002; Yoon and Kim, 2009). Because the depth of the Soya Strait is only 55 m, sea level changes could significantly affect the strength of the TWC, which can transport suspended materials downstream.

The sediment cores taken from Site U1423 extend from the Holocene to the early Pliocene and are dominated by clay, silty clay, and diatom ooze. The depth scales used during the cruise were CSF-A, CCSF-A, and CCSF-D (Tada et al., 2018). CSF-A is the depth (m) drilled from the sea floor regardless of potential gaps and overlaps between cores. Because multiple holes were drilled at U1423, the core gaps recognized at one hole were fulfilled with the corresponding interval found at an adjacent hole, and a composite depth scale (CCSF-A) was defined by adjusting the original drilled depth (CSF-A) for each hole. Splicing continuous intervals from the multi-hole sequences, a single continuous sediment sequence was established, the depth scale of which was

called CCSF-D. The sediment sequence is divided into two units based on lithology (Tada et al., 2015). Unit I (0-107 m CCSF-D) mainly consists of silty clay and clay, exhibiting cycles of dark (organic matter rich) and light (organic matter poor) colored layers. Unit II (107-240 m CCSF-D) mainly consists of diatomaceous silty clay, clay, and diatom ooze, which is homogeneous or bioturbated.

The initial stratigraphic frameworks and spliced depth scale (m CCSF-D) established onboard were mainly based on the sediments' physical properties, such as color (RGB or reflectance spectrum and colorimetry (RSC)), gamma-ray attenuation density (GRA), natural gamma-ray radiation (NGR), and magnetic susceptibility (MS). However, disturbances in the half cut core, such as Styrofoam (filled for voids and interstitial-water / paleontological sampling intervals), core liquefaction, rotated ash layers, scratched surfaces, deformations, and drilling faults, can be only recognized by visual inspection, which may lead to noises in the profile of physical properties. Such disturbed stratigraphic intervals involved in the spliced sequence could be removed and replaced with the corresponding undisturbed intervals found in the other hole. By these amendments of the original spliced sequence, a nearly continuous sequence was established (Irino et al., 2018). The revised depth scale is defined as m CCSF-D_Patched. Using this patched stratigraphic sequence, we could establish a more accurate stratigraphic framework.

Because the resolution of the initial age model is not high and one of the control points

is ambiguous (Tada et al., 2015), the age model for U1423 was also revised. U1424 is located at the southeastern margin of the Japan Basin at 40°11.40′N, 138°13.90′E (Tada et al., 2015) and is close to Site U1423. Both sites are under the influence of the first branch of the TWC. At Site U1424, GRA and NGR were tuned onto the LR04 benthic oxygen isotope stratigraphy (Lisiecki and Raymo, 2005) by Tada et al. (2018). We projected this "U1424_LR04 tuned age" to Site U1423 based on the inter-site correlation using dark - light cycles (Tada et al., 2018) from 0 to 75 m CCSF-D_Patched. From 75 m to 127 m CCSF-D_Patched, the GRA density of Site U1423 was directly tuned onto the LR04 oxygen isotope stratigraphy (Lisiecki & Raymo, 2005) (Fig. 4). We used a total of 200 control points to maintain a high resolution age model for the last 3 Myr, and the control points are shown in Figures 2 and 3 and listed in Table 2 (Lu et al., 2018). GRA at U1423 could be regarded as a proxy for sea level change in the Japan Sea because a low GRA associated with high diatom content indicates high sea level (Tada et al., 1999). Below 146.7 m CCSF-D_Patched, age control points adopted in the cruise report were used (Tada et al., 2015) (Fig. 5). The 109 samples between 0 and 200 m CCSF-D_Patched were collected for this study, which covered the last 4.3 Myr (Lu et al., 2018).

2.2. Wakasa Bay KR15-10 Sites WB6 & 8

Site WB6

Site WB6 is located in the Wakasa Basin at east of Wakasa sea knoll chain (36° 54.2898'N, 135°10.5428'E), with its water depth of around 845 m (Fig. 6). There is no evidence on its influence at the flat basin floor from the obtained sub bottom profiler.

Site WB8

Site WB8 is located at the flat sea floor in the Oki Trough (36°54.2898N', 135° 10.5428'E), which is a ENE-WSW oriented bathymetric depression in the southern Japan Sea, with its water depth of 1738 m (Fig. 6). The Oki Trough has been filled by hemipelagic mud with numerous submarine gravity flow deposits (Ikehara et al., 1990) from its southern slope.

Treatment of multiple core samples

Multiple Corer (MC) consists of frame (620 kg in weight) and eight sub-corer attachments. The sub-corer pipes made from acryl or polycarbonate are used for the sediment coring. Every time for collect samples, the wire out speed is up to 50 m/min. The MC is stopped at the depth about 30 m above the sea floor and kept for 3 minutes. After that, the wire is run out at a speed of 20 m/min. Wire tension is logged during the operation and is used for judging whether MC arrive at or leave from the sea floor. The recovered sub-corer pipes were moved into the laboratory. First, we removed the water present on the core in a plastic tube top. After the water was removed, the core was

transported to the multicore sampler supporter. Here, we pushed downward the tube until one centimeter of sediments came out from the top of the tube. At this moment, the bottom of the core tube was then stabilized using a screw driver. The sediment out from the top of the tube (1 cm) is then sampled using a spatula. During the sampling, we remove the sediments in the margin for preventing contamination. The 5 fresh samples between 0 and 5 cm were collected for this study.

2.3. Lake Suigetsu SG-12

Lake Suigetsu is one of the Mikata Five Lakes located in the southern part of the Fukui Prefecture in central Japan (Suzuki., 2016) (Fig. 7). The catchment area of Lake Suigetsu is small (8.3 km^2), and the lake water of Lake Suigetsu comes mainly from the catchment of Lake Mikata, which is connected to Lake Suigetsu by a shallow channel, only fine suspended detrital particles can reach Lake Suigetsu (Nakagawa et al., 2012; Schlolaut et al., 2014). A short gravity core named SG12-LM3 with a length of approximately 25 cm was recovered from the central part of Lake Suigetsu using a Limnos core sampler on July 6, 2012 (Kansanen et al., 1991; Suzuki et al., 2016). The accurate high resolution age model is based on radionuclide concentration and varve counts (Suzuki., 2016) (Fig. 8). The 118 data of elemental carbon (EC) concentration in the coarse (>2 μm) and fine (<2 μm) fraction for SG12 core covering the last 15 kyr were cited from Nakai (2016MS). The 15 samples out of these 118 samples between 0 and 16 m were selected for BPCA analysis in this study.

Chapter 3. Methods

3.1. Thermal optical transmittance (TOT) measurement

Sediments were freeze-dried, after which 100 mg of each sample were treated with 1.2N hydrochloric acid at room temperature overnight to remove carbonate and rinsed with milli-Q water twice to remove salts. The samples were dispersed in milli-Q water and separated into <2 μm (fine fraction) and >2 μm (coarse fraction) by the repeated settling method. The fine fractions were collected on Φ49 mm quartz fiber filters using suction filtration, while the coarse fractions were collected by centrifugation at 3000 rpm for 30 minutes followed by freeze drying and weighing (Lu et al., 2018) (Fig. 9).

The analysis was conducted using a Semi-Continuous OCEC Carbon Aerosol Analyzer manufactured by Sunset Laboratory (Miyazaki et al., 2007) at the Institute of Low Temperature Science, Hokkaido University. This apparatus is equipped with a thermal optical transmittance (TOT) system that uses a highly sensitive analytical method for determining the contents of EC. The contents of EC in both fine and coarse fractions of Site U1423 samples were measured as a proxy for biomass burning. For the fine fraction, a Φ14 mm part was punched out from the Φ49 mm quartz fiber filter and covered with another blank Φ14 mm quartz fiber filter. For the coarse fraction, a known amount (approximately 10 mg) of the freeze-dried fraction was sandwiched by two Φ14 mm quartz fiber filters. These prepared Φ14 mm quartz fiber filters were set in the

quartz glass tube of the apparatus (Fig. 10).

In this study, we used a temperature protocol based on that proposed by Miyazaki et al. (2007). A single sample was placed immediately into the apparatus. Figure 10a shows an example thermogram used in this study. The temperature was increased from room temperature to a high temperature in five steps (250℃, 350℃, 550℃, 750℃, and 850℃). The duration of each temperature step and heating rate were set as constants and routinely controlled by a computer program. The ambient environment was a complete helium atmosphere from 0 to 370 seconds at three temperature steps (250°, 350°, and 550°C) to remove non-fire resistant organic carbon (OC), and, then, from 371 to 820 seconds, the atmosphere was switched to a 2% oxygen / helium mixture at temperature steps of 550°, 750°C, and 850°C to combust the residual carbon. Carbon fractions extracted at each temperature step were detected and quantified by a Non-Dispersive Infrared (NDIR) sensor and defined as six carbon fractions from C1 to C6 (Lu et al., 2018) (Fig. 11a). From 821 seconds, a fixed volume of methane was injected into the quartz tube, providing a known quantity of carbon. The carbon amount of the introduced methane was calibrated using sucrose standards before measurement.

During the entire sequence above, laser transmission was also monitored to determine how the blackness of the sample filter changed (Lu et al., 2018) (Fig. 11a). The laser transmission data generated by the apparatus were necessary to calibrate for its temperature dependency and convert the value to a “transmission ratio”, where the laser

transmission with no carbon fraction (after the measurement sequence) was set to unity (Lu et al., 2018) (Fig. 11a). The relationship between the laser transmission and temperature can be expressed as a quadratic function (Lu et al., 2018) (Fig. 11b), where all the "black" carbon materials had been removed. The quadratic function could provide the laser transmission value anticipated at a temperature with no “black” carbon in the sample. The laser transmission at each temperature during the measurement was divided by this anticipated laser transmission value, which yielded the “transmission ratio”. Under the helium atmosphere, part of the carbon was charred, the sample became darker, and the laser transmission ratio decreased. Then, under an oxygen atmosphere, charred carbon was burned, and the laser transmission ratio was recovered to the original level (Lu et al., 2018). We defined the carbon generated from 0 seconds to this time as OC, and the carbon extracted between the time when the laser transmission was recovered to the original level and 820 seconds was regarded as EC (Lu et al., 2018) (Fig. 11a).

Analytical errors were introduced during the determination of carbon amount and the distinction of OC and EC. The uncertainty during carbon determination was ±1.8 μgC for a single measurement, whereas the error related to distinguishing OC-EC was ±0.4 μgC due to the uncertainty of the initial laser transmission. Depending on the sample amount (~10 mg and 10-30 mg for coarse and fine fractions, respectively) collected on the quartz fiber filter, the total EC determination errors were ±0.22 mgC / g sediment for the coarse fraction and ±0.7 mgC / g sediment for the fine fraction (Lu et al., 2018).

3.2. Benzene polycarboxylic acids (BPCA) measurement

For bulk sample, about 0.5 mg of finely powdered sample were weighed into glass ampules (Dittmar, 2008). After, 0.5 ml HNO_3 (65%) was added to each ampoule. Then, ampoules were flame-sealed (Bostick et al., 2018), and placed into aluminum foil sleeve that were held in a 170 ℃ furnace for 8 h (Dittmar, 2008). The aluminum foil sleeve was used to prevent a chain explosion. After oxidation, the ampoules were, and the liquid sample was filtered (Millex syringe driven filter unit, Aperture size: Φ=0.45). For standard charcoal sample, after that transferred 0.2 ml sample into 2 ml glass vials. At vials the nitric acid evaporated under a N_2 stream at 45 °C. Then the samples were redissolved in 0.5 ml of mobile phase A. The 0.5 ml solutions containing the BPCAs stored in the refrigerator until HPLC analysis (Wiedemeier et al., 2016) (Fig. 12).

For sediment sample, transferred all sample into beaker and adjust volume to 20 ml. The dilution is needed to stop further digestion (Wiedemeier et al., 2016). For each sample, prepare one glass column (300 mm height, 20 mm diameter) with 11 g of cation exchange resin (Dowex 50 W X 8, 200–400 mesh, Fluka, Steinheim, Germany) per column. The resin inside the columns is conditioned by consecutively rinsing it with: 2 column volumes of water, 1 column volume of 2 M NaOH, 2 column volumes of water for neutralizing pH, 1 column volume of 2 M HCl, and eventually 2 column volumes of water (Wiedemeier et al., 2016). The conductivity of the water, which is rinsed

through the resin after its conditioning was checked by conductivity meter. The resin is considered as properly conditioned when the conductivity is below 2 μS cm^{-1} (Wiedemeier et al., 2016). Put each sample on each column, rinse sequentially 5 times with 10 ml water. Liquid nitrogen was used to freeze the samples freeze drying for acid removal. The C18 solid phase extraction cartridges is conditioned according to the manufacturer's instruction manual, i.e., consecutively rinse them with 3 ml of methanol, 3 ml of water and eventually with 3ml of methanol/water (1:1 v/v). And redissolved the freeze dried residue in 3 ml methanol/water (1:1 v/v) (Wiedemeier et al., 2016; Miller et al., 2017). Each them (3 ml) over a separate C18 solid phase extraction is eluted cartridge into 10 ml test tubes. The cartridges was rinse with another 3 ml of methanol/water (1:1 v/v). In test tubes the methanol/water (1:1 v/v) evaporated under a N_2 stream at 45 °C. Then the samples were redissolved in 1 ml of mobile phase A. 1 ml sample was transferred into 2 ml glass vials.

BPCAs were analyzed with a Agilent HPLC system (Agilent 1260), equipped with an auto sampler, sample and column coolers, and the photodiode array absorbance detector (absorbance spectra (190–640 nm)). The chromatographic settings are same as Dittmar (2008). Quantification operated with Agilent Open LAB CDS ChemStation software. Concentration of standard solutions of BPCAs covers the range of 5 ~ 500 μM, they used to generate a calibration curve and as a reference for UV absorption spectra (Schneider et al., 2011; Miller et al., 2017). The 1,2,3,4-B4CA and 1,2,3,5-B4CA are not commercially available and the 1,2,3,4-B4CA could be an oxidation product from

benzo(a)pyrene (Dittmar, 2008), so this study was the peaks of 1,2,3,4-B4CA and 1,2,3,5-B4CA were not quantified as B4CA sum. And the results show that the 1,2,3,4-B4CA and 1,2,3,5-B4CA content is actually very low, and we do not want to increase the uncertainty of the analysis results. Only the peaks of pyromellitic acid (1,2,4,5-B4CA) were quantified as B4CA. We quantified total BC concentration of the samples as BPCA sum (Schneider et al., 2010), all the BPCA concentration data was calculated without using the conversion factor 2.27 (Glaser et al., 1998) or even higher 4.5 (Brodowski et al., 2005; Kaal et al., 2008).

Chapter 4. BPCA methods used as molecular thermometers

4.1. Preparation of standard charcoal

We agree with the judgment of the study of potential charcoal source area (PCSA) that the coarse BC comes from the local fire (Peters and Higuera, 2007; Higuera et al., 2007). And the studies on BC in deep-sea sediments have shown that ultrafine particles of BC (diameter < 2 μm) may come from remote fires (Lu et al., 2018). The fine dust generated by the Siberian forest fire can be transported long distances to the Japan Sea by means of aerosols (Lu et al., 2018). Confirmation of BPCA applicability to molecular thermometers to various plants collected in PCSA. Therefore, this study selected five different plants to quantify their thermal properties, including four Japanese native plants and one Arctic tundra plant (Table.1).

Samples of *Salix richardsonii* were collected in the Arctic tundra zone, this site is located in the Indigirka River lowland near Chokurdakh (70°38′N, 147°53′W), Russian Federation (Fan et al., 2018). Samples of *Ulmus laciniata*, *Ulmus davidiana var*, *Chamaecyparis obtusa* and *Larix kaempferi* were collected by a gardener at Hokkaido University Botanical Gardens (43°3′49.183″N, 141°20′36.179″W). *Ulmus laciniata* and *Ulmus davidiana var* are main broadleaf plants in Japan, while *Chamaecyparis obtusa* and *Larix kaempferi* are the main conifers in Japan. *Ulmus laciniata* and *Larix kaempferi* are concentrated in the northern part of the Japanese archipelago, while

Ulmus davidiana var and *Chamaecyparis obtusa* are concentrated in the southern part of the Japanese archipelago. Such a combination of plant species are intended to limited reproduce the thermal characteristics of the coarse BC produced by the local fire in the Japanese archipelago, and can be compared with the thermal characteristics of the BC of the remote fire.

Plant samples were divided into wood (branches) and leaves, which were used to make wood-charcoal and leaves-charcoal. The sample was washed with milli-Q water, dried, and pulverized. The cleaned and dried coarse particle plants samples were placed in crucible (Porcelain crucible, Coors, 30ml) and then placed in the muffle furnace (KDF Burn out furnace 007 Plus, KDF, Made in Japan) for pyrolysis. Each type of plant sample is stored in a separate crucible, even the wood and leaves samples of the same plant are heating treated separately. Before each use, the crucibles were ablated at 850 ° C for 4 hours under O_2 gas in the muffle furnace to remove organic carbon and elemental carbon on the crucible surface. The internal volume of the muffle furnace is about 2.5 liters, and the nitrogen flow rate for the furnace during pyrolysis is controlled at more than one liter per minute. The exhaust pipe of the muffle furnace is filled with quartz wool, which to further reduce the possibility of oxygen intrusion during pyrolysis. Wood-charcoal were produced from coarse wood chips (Table 1) by combustion at 240 ℃ in the muffle furnace and by pyrolysis under flowing nitrogen gas (held at peak temperature of 350, 550, and 850 ℃ for 1 hour). Using the same pyrolysis technique, leaves-charcoal was prepared for broken leaves (Table 1) at 350,

550, and 850 ℃. The muffle furnace is heated from a room temperature to 240 ° C at a rate of 60 ° C per minute, then heated from 240 ° C to the peak temperature at a rate of 2 ° C per minute. Maintain the target temperature for 1 hour to ensure complete pyrolysis of the sample. After the heating process, the sample was cooled to a room temperature under nitrogen gas and then stored in a low-density polyethylene plastic bag.

4.2. B6CA in standard charcoal

Looking at the contribution of the individual marker molecules derived from the laboratory-generated chars (Fig. 13), for wood-charcoal, the B3CA, B4CA in the 350 ° C and 550 ° C range strongly increase, but in the 850 ° C these molecules show a sharp decrease. But these rules do not apply to B5CA yield for wood-charcoal. Because we can clearly see that the B5CA at the wood-charcoal of derived from the three plants of *Salix richardsonii*, *Ulmus laciniata* and *Larix kaempferi* has a considerable yield at high temperature. This difference from the vegetation of Schneider et al., (2011b) is only one type, while in this study the introduction of a richer starting material. The relative abundance of B6CA has been associated with the highest heat treatment temperature (HTT) (Boot et al., 2015). It is true that the yield of B6CA increases with the pyrolysis temperature increase, but even at the same temperature, the yield of B6CA from the wood-charcoal of the *Chamaecyparis obtusa* and *Ulmus davidiana* are significantly lower than those of other plants. For leaves-charcoal, the B3CA, B4CA and B5CA in

the 350 ° C and 550 ° C show a high value, in the 850 ° C these marker molecules show a low value or even missing. The yield of B6CA increases with temperature increase, but this rule only applies to the leaves-charcoal of derived from the *Salix richardsonii* and *Chamaecyparis obtusa*. We quantified total BC concentration of the standard pyrolysis charcoal as BPCA sum. B5CA and B6CA are majority of BPCA sum at any time.

The relative contribution of B6CA (B6CA (%)) derived from the laboratory-generated chars are shown in Fig. 14. For wood-charcoal and leaves-charcoal, the B6CA (%) increase with increasing temperature, also they maintain max similarity. Similar to the value of B6CA (%) at 250 ~ 450 °C is about 30% (Wiedner et al., 2013) and at ~ 1000 °C is about 95% (Kaal et al., 2008; Kaal and Rumpel, 2009) . There is a little difference in the B6CA (%) value of leaves-charcoal between different plants. Even the B6CA (%) value derived from *Salix richardsonii* are only 5% higher than the local plants. The needles of *Larix kaempferi* show the weakest fire resistance, leaving only ash after pyrolysis at 850 °C. In the natural state, considering the influence of the aging of BC, B6CA relative contribution should also be the factor for evaluating fire temperature. In particular, we noticed that leaves-charcoal and wood-charcoal showed a highly consistent trend on the factor (Fig. 14). This means that the identification of the sample does not take into account the effects of leaves-charcoal (Schneider et al., 2013) or the uncertainty caused by differences between plants and regional (Fig. 15). Regardless of plant species or parts, B6CA (%) is suitable to reconstruct pyrolysis

temperature.

There are many limitations of using BPCA as a “ molecular thermometer ” to estimate the carbonization temperature of biomass BC (Schneider et al., 2013). We recommend that when using the BPCA molecular marker method to estimate wildfire temperatures, it may be preferable to use the B6CA (%) as a proxy factor. The relationship between pyrolysis temperature and B6CA (%) shows a strong positive correlation (R^2=0.94, P<0.001; Fig. 16), with an exceptional outlier with high B6CA (%) (87%, leaves). The strong positive correlation between them, pyrolysis temperature could be a first-order control on B6CA (%). Due to the differences between plants, the value of B6CA (%) is almost continuous at low-mid pyrolysis temperatures, but significantly higher at high pyrolysis temperatures (Fig. 16). The results of European plants also showed a similar trend, but showed a higher B6CA (%) in the range between 200 and 700 °C (Fig. 17). Pyrolysis temperature were estimated from B6CA (%) by the following formula:

$$\text{Pyrolysis temperature (°C)} = \text{B6CA (\%)} \times 6.95 + 295.6$$

$$R^2 = 0.94 \; P < 0.001$$

Summary

The standard charcoal combination produced under the same pyrolysis temperature sequence embodies the thermal characteristics of the coarse BC produced by the local fire in the Japanese archipelago, and can be compared with the thermal characteristics of the BC of the remote fire. B5CA and B6CA are majority of BPCA sum at any time.

Regardless of plant species or parts, B6CA (%) is suitable to reconstruct pyrolysis temperature. There is a little difference in the B6CA (%) value of leaves-charcoal between different plants. Now we can accurately reconstruct the wildfire temperature.

Chapter 5. Comparison between TOT and BPCA methods

Usually, TOT methods are not ideal for soil studies as in their methodology these incorporate the definition of BC as light-absorbing material irrespective of its origin (Hammes et al., 2008). And the BPCA method is likely to underestimate the BC content in soil samples (Dittmar, 2008). There is no systematic assessment of the potential impact of these two methods on sediment sample analysis results.

We provide TOT and BPCA analyses to assess their ability to quantitatively record BC content in various sediments. These two methods could quantifies changes in BC content (Fig. 18). However, when the BC concentration is high (eg., EC > 4.5 mg/g or BPCA > 1 mg /g), the results of the two methods show relatively large differences. The relationship between BPCA sum and Fine EC content shows a strong positive correlation ($R^2 = 0.77$, $P < 0.001$; Fig. 18), so BPCA could be mainly extracted from fine EC. Carbonation is known to occur during diagenesis (maturation) in older sediment. However, BPCA results show that the effect of carbonation on fine EC may be very limited.

The concentration of BPCA depends on the concentration of carbon in BC, and the concentration of EC is the concentration of BC itself. The EC / BPCA sum of most sediment around 2.3 ~ 4.5 (Glaser et al., 1998; Dittmar, 2008; Hammes et al., 2008), which is close to the results of the soil samples. However, we note that the EC / BPCA

sum of modern surface sediments is much higher than this, and occasionally similar high values occur in the EC / BPCA sum of surface sediments from the shallow sea is higher than that of deep sea and SG12 shows smallest EC / BPCA sum, which may be due to the differentiation of BC particles during transportation and the specific surface area. Fine particles of BC can be transported away from fire center and they have a larger specific surface area. A larger specific surface area can increase the efficiency of nitric acid oxidation, and BPCA has a higher yield. However, a further sampling and experimental analysis will be required to confirm such a grain size effect. Namely, charcoal / soot ratio may control the EC / BPCA sum, and previous studies using the BPCA method may have underestimated the BC content in the sample (soil or sediment) (Glaser et al., 1998; Kaal et al., 2008; Hammes et al., 2008; Wolf et al., 2014; Vachula et al., 2018b).

At any time or depth scales, the distribution of B3CA and B4CA did not show decreasing trend and remained fairly long time (Fig. 19). The distribution of B6CA also did not show age or depth dependent increase (Fig. 20). Concentration of BPCA sum and fine EC at Japan Sea U1423 are still high in old sediment. The concentration of BPCA varies more largely than EC in the Unit II. Therefore, significant aging effect or diagenetic decomposition of BPCAs did not occur, and the BPCA method may be more sensitive to aged samples. For long-term aging sediment samples, the BPCA method can be used to quantify the BC content better than the TOT method.

Studies on sediment samples have shown that prolonged aging of BC will cause a slight increase in the value of B6CA (%) (Hammes et al., 2008; Schneider et al., 2011a). In the known aging process, part of B3CA and B4CA are converted to B6CA, and the degree of condensation of BC is increased (Singh et al., 2014; Fischer et al., 2018). The dissolution of the unstable portion of BC leads to this result (Abiven et al., 2011). But the contents of unstable part of BC is very low (Zimmerman, 2010; Stewart et al., 2013; Zimmerman and Gao, 2013), moreover, the value of B3CA and B4CA relative contribution in environmental matrix samples is not significantly high (Schneider et al., 2010; Schneider et al., 2011a; Boot et al., 2015). The values of B6CA (%) for fresh BC and aged BC are shown in Figure 20. The effect of aging on B6CA (%) was not significant, this also means pyrolysis temperature of BC could estimate from B6CA (%).

Summary

TOT and BPCA methods could quantifies changes in BC content. The specific surface area of BC may have a potential effect on the yield of PBCA during nitric acid oxidation. So charcoal / soot ratio may control the EC / BPCA sum. For long-term aging sediment samples, the BPCA method can be used to quantify the BC content better than the TOT method. The effect of aging on B6CA (%) was not significant, this also means pyrolysis temperature of BC could estimate from B6CA (%).

Chapter 6. Application to sediment archives

In this study we provide TOT and BPCA analyses to assess their ability to reconstruction of biomass burning magnitude, temperature and evaluation of fine BC in the past.

6.1. Application to surface marine sediment

The surface sediments from Wakasa Bay show very low concentration of BPCA and EC, despite this, the far away from land site (WB8) is have a higher concentration of BPCA and EC than the close to land site (WB6). EC fine fraction are only appear at the top once, while the majorities are coarse fraction (Fig. 19). The thermal characteristics indicate that the combustion temperature of BC at WB6 is much lower than WB8 (Fig. 21).

High-temperature forest fires emit more submicron diameter soot (Masiello, 2004; Thevenon et al., 2010) that can be quickly transported by wind to very long distances (Masiello, 2004). In contrast, low-temperature forest fires emit more large-diameter charcoal (Masiello, 2004; Thevenon et al., 2010), most of which are slowly transported over water to distant locations (Clark, 1988; Whitlock and Millspaugh, 1996; Ohlson and Tryterud, 2000; Scott, 2010). Unlike Lake Suigetsu's stable immersion environment, Japan Sea's submarine terrain has a large depth variation over very short

distances, and the water flow rate is much faster than Lake Suigetsu. This also explains the low content of fine EC in the sediments of Wakasa Bay and U1423. This phenomenon at surface marine sediment may be explained by the differentiation of BC during transport due to particle diameter. But at this stage we don't have enough evidence (such as stable isotope) to prove that WB6 and WB8 share the same stable fire center area for a long time. Considering that fine particle BC may come from remote fire sources (Lu et al., 2018), there is another assumption that the BCs of WB6 and WB8 are from different fire center areas.

6.2. Application to deep marine sediment

The contents of EC are higher than 3 mg / g in Unit I (0 – 2.2 Ma) and lower than 2 mg / g in Unit II (2.2–4.3 Ma). While, the contents of BPCA are higher than 0.5 mg / g in Unit I and Unit II. The contents of BPCA sum and EC during the last 4.3 Myr at Site U1423 are shown in Figure 22. The contents of BPCA sum and EC are high in Subunit IA (0-1.8 Ma) and decrease rapidly downward in the upper part of Subunit IB (1.8-2.2 Ma). BPCA sum content is still high in unit II, but low levels of EC content are maintained in Subunits IIA (2.2-3.0 Ma) and IIB (>3.0 Ma). EC in the coarse (> 2 μm) fraction are 5-10 times higher than those in the fine (< 2 μm) fraction. The content of coarse EC is steady in Subunit IIB (>3.0 Ma), whereas the contents of BPCA sum and fine EC shows significant fluctuations in the same subunit. The BPCA sum content showed two frequent biomass burnings at 2.3 Ma and 3.7 Ma, but the total EC content

only showed very limited biomass burning at same.

Fine EC content varies independently from coarse EC content (Fig. 22), which suggests a remote origin of fine EC. The fine particles of EC might be transported out of a fire site by wind, which is different from coarse EC (Scott, 2010). In particular, canopy fires can produce fine EC particles that are susceptible to wind dispersal. Taking into account the fact that the fine particles could be transported over long distances as aerosols, unusually high contents of fine EC suggest contributions from remote fires. Wildfires occur mainly in spring and autumn in East Asia because fires are mostly triggered by a sudden change in environment, such as sudden changes in humidity and ignition probability. Usually autumn and late winter or early spring experience numerous wildfires. This time is same as Asian dust, which is originates in China, Mongolia or Kazakhstan where high-speed surface winds and intense dust storms kick up dense clouds of fine, dry soil particles. Therefore, fine EC and Asian dust could have similar transport processes. Based on modern aerosol research (Huang et al., 2011; Huang et al., 2014) and high-resolution variations in aeolian dust research (Irino and Tada, 2003), eastern and northwest China and Mongolia could be sources of fine EC. The ratio of coarse EC and fine EC changes over time due to the potentially wider range of fire source areas which are affected by the East Asian monsoon. Strong westerly winds can carry large amounts of fine particulate matter over long distances and could finally deposit them in the Japan Sea (Lu et al., 2018). Considering that the main BPCA is derived from fine EC, it is possible that remote fires are very frequent at 2.3 Ma and

3.7 Ma.

Our high-resolution age model covers the last 3 Myr, which enables us to examine the relationship between EC grain size and glacial - interglacial cycles. The maxima events in fine EC / coarse EC occurred during interglacial intervals. In interglacial stages, large-scale terrestrial vegetation could provide ample loads of fuel and higher chances for ignition events, where lightning might be a main ignition event (Marlon et al. 2013). These conditions could provide the possibility of large-scale biomass burning, which could generate fine elemental carbon in East Asia. We note that the high interglacial precipitation was not sufficiently powerful to drive a linear change in local fires, and their correlation was weak. When precipitation exceeded a threshold, it may suppressed or promoted fires. However, it is difficult to quantify this threshold simply by relying on current pollen data. Such large-scale biomass burning at a remote fire site could have served as a fine EC supply for Site U1423 (Lu et al., 2018).

A set of second-highest peaks of Fine EC / Coarse EC appeared in the glacial stages, which were found during 267~279 ka and 358~370 ka (Fig. 22). Lower peaks also appeared in the glacial stages, which were found during 1.60~1.63 Ma and 2.11~2.13 Ma. Under normal circumstances, the amount of coarse EC is much higher than that for fine EC. Changes in wind strength could significantly affect fine EC flux. Therefore, these exceptionally high fine EC contents suggest a special condition of enhanced winds during particular glacial stages, which corresponded to MIS 8, MIS 10, MIS 56

and MIS 80 (Lu et al., 2018).

The strong winds during glacial stages could carry great amounts of terrigenous clastic particles, which could cause abnormal increases in the contents of certain terrestrial substances, such as freshwater diatoms (Pokras and Mix, 1987)(Verardo and Ruddiman, 1996). Researches for modern aerosol (Han et al., 2008; Wang et al., 2012; Huang et al., 2014) and past aeolian dust variability showed that source of fine terrigenous clastic particles in the north Pacific was central and northern Eurasia, and their flux could be a proxy for the continental aridity or the length of dust season (Irino and Tada 2003). During the glacial period, the surface of mainland China was heavily weathered, and a large number of debris particles were formed. Under the influence of strong winds, this newborn terrigenous clastic debris could have been transported into the ocean. The wind strength or direction during glacial stages could also affect the change in tempo of charcoal deposition. The biomass burning was relatively stable on the loess plateau (Zhou et al., 2007) for MIS 8 and MIS 10. Coarse particle content increased significantly on the loess plateau at MIS 8 and MIS 10 (Sun et al., 2003), and, at the same time, the mean grain size of bulk sample data also indicates a stronger East Asian winter monsoon (Sun et al., 2006). Based on particle sizes and the magnetic susceptibility of the Loess Plateau, weaker summer and stronger winter monsoons were suggested during MIS 8 and MIS 10 (Wang, 2003)(Hao et al., 2012). At MIS 56 and MIS 80, the magnetic susceptibility of the Loess Plateau shows a slightly stronger winter monsoon (Nie et al., 2008). Although the fine EC concentration increased during

those particular glacial phases, it does not necessarily mean that the biomass burning or fuel load had increased. The strong winds could have carried land-deposited EC particles into the ocean (Lu et al., 2018). Benefitting from the strong winter monsoon in the surrounding area, larger supplies of fine EC to Site U1423 could have been realized during MIS 8, MIS 10, MIS 56 and MIS 80.

The pollen assemblage could reveal more information on vegetation and climate. Here, we compared our EC analysis results with pollen data collected from the same sample set (Igarashi et al., 2018). The total pollen number was a proxy for the volume of terrestrial vegetation that could be a major part of biomass fuel load for fires. The relationship between pollen count and coarse EC content shows a weak positive correlation (R^2=0.417, P<0.001; Fig. 23), with an exceptional outlier with high pollen number (92022 /g) and low coarse EC (0.689 mg/g). Despite the weak positive correlation between them, a larger biomass or high biomass fuel load could be a first-order control on coarse EC supply (Lu et al., 2018). The very high coarse EC content and the great number of pollen or very high precipitation were sometimes unsynchronized. In the case of high coarse EC associated with low precipitation, a time lag between EC generation and transport might be responsible (Lu et al., 2018). The relationship between total number of pollen and fine EC content shows no significant correlation (Fig. 24).

Data based on total pollen number shows that high values for volume of terrestrial

vegetation occur in interglacial periods (Fig. 25). And the fire temperature estimated from B6CA (%) indicate that they have frequent high temperature fire events in interglacial periods, while the low temperature fire events in glacial periods (Fig. 26). Ordinary temperatures in biomass burning are approximately 400 °C, whereas canopy fires can be much hotter (more than 800°C; Scott, 2010). Usually in terms of local fires, the four conditions of resin content, wind speed, water content, and carbonization time determine the specific fire temperature (Archibold et al., 1998; Hoesel et al., 2012; Wolf et al., 2013). But with a longer time scale and a wider range of sources, the biomass fuel loads controls changes in fire temperature. Studies of modern forest fires have shown that woody plants have an average burning temperature far exceeding that of shrubs and herbs (Wolf et al., 2013). The bark of the coniferous forest is thicker and more resistant to fire, while the broad-leaved forest has more flammable resin and burns at a higher temperature (Schneider et al., 2013). Finally, usually high temperature forest fires are caused by lightning (Scott, 2000; Krawchuk et al., 2009; Marlon et al., 2013). Resin-rich broad-leaved forests were frequently ignited by lightning, such these fire zones could provide a stable high temperature BC. These facts (Fig. 26) suggest that high-temperature paleofires occurred more frequently during interglacial stages in Northern Asia. Because, burning at high temperatures with high level of biomass fuel loads is difficult in a cold and dry environment. The sizes of biomass fuel loads during glacial times might have been very small and were insufficient for large-scale biomass burning or high-temperature burning (Lu et al., 2018).

6.3. Application to lake sediment

The younger sediments from Lake Suigetsu (SG12) have high concentration of BPCA and EC. BPCA sum and Fine EC was dominated during the early stage (15~10 ka), and coarse EC increased during the later stage (10~0 ka) (Fig. 27). Local fires supplied the majority of coarse charcoal at the later stage (Clark, 1988; Whitlock and Millspaugh, 1996; Clark et al., 1998; Ohlson and Tryterud, 2000; Scott, 2010). The high coarse EC content at 4 ka may be derived from increased human activity (Nakai, 2016MS). Based on pollen data shows that this area is warm (Demske et al., 2013), the nearby Lake Biwa also showed high concentration of TOC accumulation at this time (Urabe et al., 2014). Referring to the results of macroscopic charcoal and pollen research in nearby Lake Biwa (Inoue et al., 2018), the significant increase in human activities by Lake Suigetsu during the 4 ka lead to an increase in the supply of large local EC, and significant changes in local vegetation, and a significant increase in the frequency of flood events (Nakagawa et al., 2012; Schlolaut et al., 2014). The high concentration of BPCA sum and fine EC in the early stage (15~10 ka) benefited from the supply of remote fires, which was the high fuel load at the remote fire point at that time.

The Chinese stalagmite data is the agent of East Asian summer monsoon (EASM) intensity (Cheng et al., 2016). The fire temperature estimated from B6CA (%) indicate that they have frequent high temperature fire events in EASM strong periods, while the low temperature fire events in EASM weak periods (Fig. 28). When EASM is strong,

East Asia is warm and humid (Xiao et al., 1999; An et al., 2006; Sun et al., 2006; Zhou et al., 2007; Guo et al., 2009; Gong et al., 2015; Bowman et al., 2011), and the fuel load is relatively high, which is more conducive to high-temperature fire events. We also noticed that although the fire temperature in the 6~9 ka phase was kept at a high position, there was no high temperature fire event (Fig. 28), at which time EASM maintained strong intensity for a long period of time. This may be due to the fact that long-term continuous precipitation induced frequent local flood events (Nakagawa et al., 2012; Schlolaut et al., 2014) that inhibited high-temperature fire events. Extremely high precipitation will inhibit the occurrence of local fires (Marlon et al., 2012; Marlon et al., 2013; Blarquez et al., 2014; Lu et al., 2018), which is also reflected in the reduction of coarse EC concentration (Fig. 27). The rule is consistent with the performance of U1423, which means that the fuel load and the wildfire temperature are positively correlated.

Summary

Fire temperature of soot was higher during interglacial periods for the last 4.3 Myr. Fire temperature of soot was higher during stronger East Asian summer monsoon periods for the last 15 kyr. The volume of terrestrial plants (fuel loads) could be a main controlling factor of fire intensity, which affected the burning temperature.

Chapter 7. Conclusions

In this study, the author compared the thermal characteristics of TOT and BPCA methods, constructed a molecular thermometer to various plants collected in east Asia, examine the aging effect, and, then, reconsted the biomass burning magnitude / temperature for various sediment archives.

7-1 Evaluation of the consistency between TOT and BPCA methods for BC quantification

TOT and BPCA methods could quantifies changes in BC content although it turned out that BPCA could be mainly originated from fine EC. Charcoal/Soot ratio may control the EC/ BPCA sum.

7-2 Confirmation of BPCA applicability as a molecular thermometer to various plants collected in east Asia

B6CA (%) consistently depends on burning temperature regardless of plant species and their parts (stems and leaves). Therefore, B6CA% could be used as "molecular thermometers" for east Asian plants as well.

7-3 Examination of the aging effect on old sediment archives (> 1 Million years)

No depth dependent trends in content and composition of BPCA as well as fine EC content were recognized even in the deep sediment core from IODP Site U1423. This

fact strongly suggests that an aging effect are not significant for BPCA and fine EC in old sediment archives.

7-4 Reconstruction of biomass burning magnitude, temperature, and fine BC emission in east Asian region in the past.

Application of TOT and BPCA methods to various sediment archives around Japanese islands revealed that;

(1) Fire temperature was higher during interglacial periods for the last 4.3 Myr

(2) Fire temperature was higher during stronger East Asian summer monsoon periods for the last 15 kyr

(3) These two observations suggest that the volume of terrestrial plants (fuel loads) could be a main controlling factor of fire intensity, which affected the burning temperature.

Acknowledgements

The research included in master thesis could not been performed without the assistance and support of many advisors and good friends. I would like to extend my gratitude to my supervisor Prof. Tomohisa Irino of Hokkaido University. He has directed me throughout my experiment, analysis and thesis with his knowledge, patience and experience.

I appreciate Dr. Yaeko Igarashi for her providing pollen data. Many thanks go to Profs. Atsuko Sugimoto, Hisayuki Yoshikawa, Yoshito Chikaraishi, Masanobu Yamamoto and Youhei Yamashita, for their reviews and comments. Many thanks also go to Profs. Kimitaka Kawamura, Yuzo Miyazaki for allowing me to use thermal optical transmittance (TOT) system.

I also thank Prof. Ryuji Tada (University of Tokyo), Dr. Ken Ikehara (AIST), Dr. Yoshimi Kubota (NMNS), Prof. Satoshi Takahashi (University of Tokyo), Prof. Takuya Sagawa (Kanazawa University) and Dr. Yoshiaki Suzuki (Geological survey of Japan, AIST) for the help and support during KR15-10 cruise and sampling party.

Prof. Takayuki Azuma (Botanic Garden, Hokkaido University) kindly provide various plant samples. I am so grateful to Dr. Rong Fan during this study as well as the members of Hensen seminar at Hokkaido University for their helpful comments and suggestions.

Finally, I would like to extend my deepest gratitude to my parents who always love and understand me.

References

Abiven, S., Hengartner, P., Schneider, M.P.W., Singh, N., Schmidt, M.W.I., 2011. Pyrogenic carbon soluble fraction is larger and more aromatic in aged charcoal than in fresh charcoal. Soil Biology and Biochemistry 43, 1615–1617. https://doi.org/10.1016/j.soilbio.2011.03.027

An, C.-B., Feng, Z.-D., Barton, L., 2006. Dry or humid? Mid-Holocene humidity changes in arid and semi-arid China. Quaternary Science Reviews 25, 351–361. https://doi.org/10.1016/j.quascirev.2005.03.013

Archibald, S., Staver, A.C., Levin, S.A., 2012. Evolution of human-driven fire regimes in Africa. Proceedings of the National Academy of Sciences 109, 847–852. https://doi.org/10.1073/pnas.1118648109

Archibold, O.W., Nelson, L.J., Ripley, E.A., Delanoy, L., 1998. Fire temperatures in plant communities of the northern mixed prairie. Canadian Field-Naturalist 112, 234–240.

Black, B.A., Sydeman, W.J., Frank, D.C., Griffin, D., Stahle, D.W., Garcia-Reyes, M., Rykaczewski, R.R., Bograd, S.J., Peterson, W.T., 2014. Six centuries of variability and extremes in a coupled marine-terrestrial ecosystem. Science 345, 1498–1502. https://doi.org/10.1126/science.1253209

Blarquez, O., Vannière, B., Marlon, J.R., Daniau, A.-L., Power, M.J., Brewer, S., Bartlein, P.J., 2014. paleofire: An R package to analyse sedimentary charcoal records from the Global Charcoal Database to reconstruct past biomass burning. Computers & Geosciences 72, 255–261. https://doi.org/10.1016/j.cageo.2014.07.020

Bond, T.C., Bergstrom, R.W., 2006. Light Absorption by Carbonaceous Particles: An Investigative Review. Aerosol Science and Technology 40, 27–67. https://doi.org/10.1080/02786820500421521

Bond, T.C., Doherty, S.J., Fahey, D.W., Forster, P.M., Berntsen, T., DeAngelo, B.J., Flanner, M.G., Ghan, S., Kärcher, B., Koch, D., Kinne, S., Kondo, Y., Quinn, P.K., Sarofim, M.C., Schultz, M.G., Schulz, M., Venkataraman, C., Zhang, H., Zhang, S., Bellouin, N., Guttikunda, S.K., Hopke, P.K., Jacobson, M.Z., Kaiser, J.W., Klimont, Z., Lohmann, U., Schwarz, J.P., Shindell, D., Storelvmo, T., Warren, S.G., Zender, C.S., 2013. Bounding the role of black carbon in the climate system: A scientific assessment. Journal of Geophysical Research: Atmospheres 118, 5380–5552. https://doi.org/10.1002/jgrd.50171

Boot, C.M., Haddix, M., Paustian, K., Cotrufo, M.F., 2015. Distribution of black carbon in ponderosa pine forest floor and soils following the High Park wildfire. Biogeosciences 12, 3029–3039. https://doi.org/10.5194/bg-12-3029-2015

Bostick, K.W., Zimmerman, A.R., Wozniak, Andrew.S., Mitra, S., Hatcher, P.G., 2018. Production and Composition of Pyrogenic Dissolved Organic Matter From a Logical Series of Laboratory-Generated Chars. Frontiers in Earth Science 6. https://doi.org/10.3389/feart.2018.00043

Bowman, D.M.J.S., Balch, J., Artaxo, P., Bond, W.J., Cochrane, M.A., D'Antonio, C.M., DeFries, R., Johnston, F.H., Keeley, J.E., Krawchuk, M.A., Kull, C.A.,

Mack, M., Moritz, M.A., Pyne, S., Roos, C.I., Scott, A.C., Sodhi, N.S., Swetnam, T.W., 2011. The human dimension of fire regimes on Earth: The human dimension of fire regimes on Earth. Journal of Biogeography 38, 2223–2236. https://doi.org/10.1111/j.1365-2699.2011.02595.x

Bowman, D.M.J.S., Balch, J.K., Artaxo, P., Bond, W.J., Carlson, J.M., Cochrane, M.A., D'Antonio, C.M., DeFries, R.S., Doyle, J.C., Harrison, S.P., Johnston, F.H., Keeley, J.E., Krawchuk, M.A., Kull, C.A., Marston, J.B., Moritz, M.A., Prentice, I.C., Roos, C.I., Scott, A.C., Swetnam, T.W., Werf, G.R. van der, Pyne, S.J., 2009. Fire in the Earth System. Science 324, 481–484. https://doi.org/10.1126/science.1163886

Brodowski, S., Rodionov, A., Haumaier, L., Glaser, B., Amelung, W., 2005. Revised black carbon assessment using benzene polycarboxylic acids. Organic Geochemistry 36, 1299–1310. https://doi.org/10.1016/j.orggeochem.2005.03.011

Buseck, P.R., Adachi, K., Gelencsér, A., Tompa, É., Pósfai, M., 2014. Ns-Soot: A Material-Based Term for Strongly Light-Absorbing Carbonaceous Particles. Aerosol Science and Technology 48, 777–788. https://doi.org/10.1080/02786826.2014.919374

Chakrabarty, R.K., Beres, N.D., Moosmüller, H., China, S., Mazzoleni, C., Dubey, M.K., Liu, L., Mishchenko, M.I., 2015. Soot superaggregates from flaming wildfires and their direct radiative forcing. Scientific Reports 4. https://doi.org/10.1038/srep05508

Cheng, H., Edwards, R.L., Sinha, A., Spötl, C., Yi, L., Chen, S., Kelly, M., Kathayat, G., Wang, X., Li, X., Kong, X., Wang, Y., Ning, Y., Zhang, H., 2016. The Asian monsoon over the past 640,000 years and ice age terminations. Nature 534, 640–646. https://doi.org/10.1038/nature18591

Clark, J.S., 1988. Particle motion and the theory of charcoal analysis: Source area, transport, deposition, and sampling. Quaternary Research 30, 67–80. https://doi.org/10.1016/0033-5894(88)90088-9

Clark, J.S., Lynch, J., Stocks, B.J., Goldammer, J.G., 1998. Relationships between charcoal particles in air and sediments in west-central Siberia. The Holocene 8, 19–29. https://doi.org/10.1191/095968398672501165

Cohen-Ofri, I., Weiner, L., Boaretto, E., Mintz, G., Weiner, S., 2006. Modern and fossil charcoal: aspects of structure and diagenesis. Journal of Archaeological Science 33, 428–439. https://doi.org/10.1016/j.jas.2005.08.008

Czimczik, C.I., Masiello, C.A., 2007. Controls on black carbon storage in soils: BLACK CARBON IN SOILS. Global Biogeochemical Cycles 21, n/a-n/a. https://doi.org/10.1029/2006GB002798

Daniau, A.-L., Bartlein, P.J., Harrison, S.P., Prentice, I.C., Brewer, S., Friedlingstein, P., Harrison-Prentice, T.I., Inoue, J., Izumi, K., Marlon, J.R., Mooney, S., Power, M.J., Stevenson, J., Tinner, W., Andrič, M., Atanassova, J., Behling, H., Black, M., Blarquez, O., Brown, K.J., Carcaillet, C., Colhoun, E.A., Colombaroli, D., Davis, B.A.S., D'Costa, D., Dodson, J., Dupont, L., Eshetu, Z., Gavin, D.G., Genries, A., Haberle, S., Hallett, D.J., Hope, G., Horn, S.P., Kassa, T.G.,

Katamura, F., Kennedy, L.M., Kershaw, P., Krivonogov, S., Long, C., Magri, D., Marinova, E., McKenzie, G.M., Moreno, P.I., Moss, P., Neumann, F.H., Norström, E., Paitre, C., Rius, D., Roberts, N., Robinson, G.S., Sasaki, N., Scott, L., Takahara, H., Terwilliger, V., Thevenon, F., Turner, R., Valsecchi, V.G., Vannière, B., Walsh, M., Williams, N., Zhang, Y., 2012. Predictability of biomass burning in response to climate changes: Biomass burning and climate changes. Global Biogeochemical Cycles 26, n/a-n/a. https://doi.org/10.1029/2011GB004249

Demske, D., Tarasov, P.E., Nakagawa, T., 2013. Atlas of pollen, spores and further non-pollen palynomorphs recorded in the glacial-interglacial late Quaternary sediments of Lake Suigetsu, central Japan. Quaternary International 290–291, 164–238. https://doi.org/10.1016/j.quaint.2012.02.002

Dittmar, T., 2008. The molecular level determination of black carbon in marine dissolved organic matter. Organic Geochemistry 39, 396–407. https://doi.org/10.1016/j.orggeochem.2008.01.015

Enache, M.D., Cumming, B.F., 2006. Tracking recorded fires using charcoal morphology from the sedimentary sequence of Prosser Lake, British Columbia (Canada). Quaternary Research 65, 282–292. https://doi.org/10.1016/j.yqres.2005.09.003

Fan, R., Morozumi, T., Maximov, T.C., Sugimoto, A., 2018. Effect of floods on the δ^{13}C values in plant leaves: a study of willows in Northeastern Siberia. PeerJ 6, e5374. https://doi.org/10.7717/peerj.5374

Fierro, A., Rutigliano, F.A., Marco, A.D., Castaldi, S., Santo, A.V.D., 2007. Post-fire stimulation of soil biogenic emission of CO2 in a sandy soil of a Mediterranean shrubland. Int. J. Wildland Fire 16, 573–583. https://doi.org/10.1071/WF06114

Fischer, D., Erben, G., Dunst, G., Glaser, B., 2018. Dynamics of labile and stable carbon and priming effects during composting of sludge and lop mixtures amended with low and high amounts of biochar. Waste Management 78, 880–893. https://doi.org/10.1016/j.wasman.2018.06.056

Glaser, B., Amelung, W., 2003. Pyrogenic carbon in native grassland soils along a climosequence in North America: C_{pyr} In north american prairie soils. Global Biogeochemical Cycles 17, n/a-n/a. https://doi.org/10.1029/2002GB002019

Glaser, B., Haumaier, L., Guggenberger, G., Zech, W., 1998. Black carbon in soils: the use of benzenecarboxylic acids as specific markers. Organic Geochemistry 29, 811–819. https://doi.org/10.1016/S0146-6380(98)00194-6

Gong, H., Zhang, R., Yue, L., Zhang, Y., Li, J., 2015. Magnetic fabric from Red clay sediments in the Chinese Loess Plateau. Scientific Reports 5. https://doi.org/10.1038/srep09706

Grosjean, D., Williams, E.L., Grosjean, E., Novakov, T., 1994. Evolved Gas Analysis of Secondary Organic Aerosols. Aerosol Science and Technology 21, 306–324. https://doi.org/10.1080/02786829408959718

Guggenberger, G., Rodionov, A., Shibistova, O., Grabe, M., Kasansky, O.A., Fuchs, H., Mikheyeva, N., Zrazhevskaya, G., Flessa, H., 2008. Storage and mobility of black carbon in permafrost soils of the forest tundra ecotone in Northern Siberia.

Global Change Biology 14, 1367–1381. https://doi.org/10.1111/j.1365-2486.2008.01568.x

Guo, Z.T., Berger, A., Yin, Q.Z., Qin, L., 2009. Strong asymmetry of hemispheric climates during MIS-13 inferred from correlating China loess and Antarctica ice records. Clim. Past 11.

GUSTAFSSON, O.R., GSCHWEND, P.M., n.d. The flux of black carbon to surface sediments on the New England continental shelf 8.

Hammes, K., Schmidt, M.W.I., Smernik, R.J., Currie, L.A., Ball, W.P., Nguyen, T.H., Louchouarn, P., Houel, S., Gustafsson, Ö., Elmquist, M., Cornelissen, G., Skjemstad, J.O., Masiello, C.A., Song, J., Peng, P., Mitra, S., Dunn, J.C., Hatcher, P.G., Hockaday, W.C., Smith, D.M., Hartkopf-Fröder, C., Böhmer, A., Lüer, B., Huebert, B.J., Amelung, W., Brodowski, S., Huang, L., Zhang, W., Gschwend, P.M., Flores-Cervantes, D.X., Largeau, C., Rouzaud, J.-N., Rumpel, C., Guggenberger, G., Kaiser, K., Rodionov, A., Gonzalez-Vila, F.J., Gonzalez-Perez, J.A., Rosa, J.M. de la, Manning, D.A.C., López-Capél, E., Ding, L., 2007. Comparison of quantification methods to measure fire-derived (black/elemental) carbon in soils and sediments using reference materials from soil, water, sediment and the atmosphere. Global Biogeochemical Cycles 21. https://doi.org/10.1029/2006GB002914

Hammes, K., Torn, M.S., Lapenas, A.G., Schmidt, M.W.I., 2008. Centennial black carbon turnover observed in a Russian steppe soil 12.

Hao, Q., Wang, L., Oldfield, F., Peng, S., Qin, L., Song, Y., Xu, B., Qiao, Y., Bloemendal, J., Guo, Z., 2012. Delayed build-up of Arctic ice sheets during 400,000-year minima in insolation variability. Nature 490, 393–396. https://doi.org/10.1038/nature11493

Higuera, P.E., Peters, M.E., Brubaker, L.B., Gavin, D.G., 2007. Understanding the origin and analysis of sediment-charcoal records with a simulation model. Quaternary Science Reviews 26, 1790–1809. https://doi.org/10.1016/j.quascirev.2007.03.010

Higuera, P.E., Whitlock, C., Gage, J.A., 2011. Linking tree-ring and sediment-charcoal records to reconstruct fire occurrence and area burned in subalpine forests of Yellowstone National Park, USA. The Holocene 21, 327–341. https://doi.org/10.1177/0959683610374882

Hodnebrog, Ø., Myhre, G., Forster, P.M., Sillmann, J., Samset, B.H., 2016. Local biomass burning is a dominant cause of the observed precipitation reduction in southern Africa. Nature Communications 7, 11236. https://doi.org/10.1038/ncomms11236

Hoesel, A. van, Hoek, W.Z., Braadbaart, F., Plicht, J. van der, Pennock, G.M., Drury, M.R., 2012. Nanodiamonds and wildfire evidence in the Usselo horizon postdate the Allerød-Younger Dryas boundary. PNAS 109, 7648–7653. https://doi.org/10.1073/pnas.1120950109

Huang, E., Tian, J., Steinke, S., 2011. Millennial-scale dynamics of the winter cold tongue in the southern South China Sea over the past 26 ka and the East Asian winter monsoon. Quaternary Research 75, 196–204.

https://doi.org/10.1016/j.yqres.2010.08.014
Huang, J., Wang, T., Wang, W., Li, Z., Yan, H., 2014. Climate effects of dust aerosols over East Asian arid and semiarid regions: Climate effects of East Asian dust. Journal of Geophysical Research: Atmospheres 119, 11,398-11,416. https://doi.org/10.1002/2014JD021796
Igarashi, Y., Irino, T., Sawada, K., Song, L., Furota, S., 2018. Fluctuations in the East Asian monsoon recorded by pollen assemblages in sediments from the Japan Sea off the southwestern coast of Hokkaido, Japan, from 4.3 Ma to the present. Global and Planetary Change 163, 1–9. https://doi.org/10.1016/j.gloplacha.2018.02.001
Inoue, J., Okuyama, C., Takemura, K., 2018. Long-term fire activity under the East Asian monsoon responding to spring insolation, vegetation type, global climate, and human impact inferred from charcoal records in Lake Biwa sediments in central Japan. Quaternary Science Reviews 179, 59–68. https://doi.org/10.1016/j.quascirev.2017.11.007
Irino, T., Tada, R., 2003. High-resolution reconstruction of variation in aeolian dust (Kosa) deposition at ODP site 797, the Japan Sea, during the last 200 ka. Global and Planetary Change 35, 143–156. https://doi.org/10.1016/S0921-8181(02)00135-2
Irino, T., Tada, R., Ikehara, K., Sagawa, T., Karasuda, A., Kurokawa, S., Seki, A., Lu, S., 2018. Construction of perfectly continuous records of physical properties for dark-light sediment sequences collected from the Japan Sea during Integrated Ocean Drilling Program Expedition 346 and their potential utilities as paleoceanographic studies. Progress in Earth and Planetary Science 5. https://doi.org/10.1186/s40645-018-0176-7
Kaal, J., Brodowski, S., Baldock, J.A., Nierop, K.G.J., Cortizas, A.M., 2008. Characterisation of aged black carbon using pyrolysis-GC/MS, thermally assisted hydrolysis and methylation (THM), direct and cross-polarisation 13C nuclear magnetic resonance (DP/CP NMR) and the benzenepolycarboxylic acid (BPCA) method. Organic Geochemistry 39, 1415–1426. https://doi.org/10.1016/j.orggeochem.2008.06.011
Kaal, J., Rumpel, C., 2009. Can pyrolysis-GC/MS be used to estimate the degree of thermal alteration of black carbon? Organic Geochemistry 40, 1179–1187. https://doi.org/10.1016/j.orggeochem.2009.09.002
Kansanen, P.H., Jaakkola, T., Kulmala, S., Suutarinen, R., 1991. Sedimentation and distribution of gamma-emitting radionuclides in bottom sediments of southern Lake Päijänne, Finland, after the Chernobyl accident. Hydrobiologia 222, 121–140. https://doi.org/10.1007/BF00006100
Kelly, R., Chipman, M.L., Higuera, P.E., Stefanova, I., Brubaker, L.B., Hu, F.S., 2013. Recent burning of boreal forests exceeds fire regime limits of the past 10,000 years. Proceedings of the National Academy of Sciences 110, 13055–13060. https://doi.org/10.1073/pnas.1305069110
Ken I., Mikio S., Hirofumi Y., 1990. Sedimentation in the Oki Trough, southern Japan Sea, as revealed by high resolution seismic records(3.5 kHz echograms). The

Journal of the Geological Society of Japan 96, 37–49. https://doi.org/10.5575/geosoc.96.37

Khan, A.L., n.d. Quantifying Sources, Distribution, and Processing of Light Absorbing Aerosols in the Cryosphere: a Comparison of Dissolved and Refractory Black Carbon in Polar and High Mountain Regions 122.

Krawchuk, M.A., Moritz, M.A., Parisien, M.-A., Dorn, J.V., Hayhoe, K., 2009. Global Pyrogeography: the Current and Future Distribution of Wildfire. PLOS ONE 4, e5102. https://doi.org/10.1371/journal.pone.0005102

Lehmann, C.E.R., Anderson, T.M., Sankaran, M., Higgins, S.I., Archibald, S., Hoffmann, W.A., Hanan, N.P., Williams, R.J., Fensham, R.J., Felfili, J., Hutley, L.B., Ratnam, J., San Jose, J., Montes, R., Franklin, D., Russell-Smith, J., Ryan, C.M., Durigan, G., Hiernaux, P., Haidar, R., Bowman, D.M.J.S., Bond, W.J., 2014. Savanna Vegetation-Fire-Climate Relationships Differ Among Continents. Science 343, 548–552. https://doi.org/10.1126/science.1247355

Li, Y., Ye, D., Sun, Z., 2017. Robust finite time control algorithm for satellite attitude control. Aerospace Science and Technology 68, 46–57. https://doi.org/10.1016/j.ast.2017.05.014

Lisiecki, L.E., Raymo, M.E., 2005. A Pliocene-Pleistocene stack of 57 globally distributed benthic δ^{18}O records: Pliocene-pleistocene benthic stack. Paleoceanography 20, n/a-n/a. https://doi.org/10.1029/2004PA001071

Lu, S., Irino, T., Igarashi, Y., 2018. Biomass burning history in East Asia during the last 4 million years recorded in elemental carbon variability at IODP site U1423. Progress in Earth and Planetary Science 5. https://doi.org/10.1186/s40645-018-0206-5

Lu, X., Cao, L., Wang, H., Peng, W., Xing, J., Wang, S., Cai, S., Shen, B., Yang, Q., Nielsen, C.P., McElroy, M.B., 2019. Gasification of coal and biomass as a net carbon-negative power source for environment-friendly electricity generation in China. PNAS 116, 8206–8213. https://doi.org/10.1073/pnas.1812239116

Lützow, M. v, Kögel-Knabner, I., Ekschmitt, K., Matzner, E., Guggenberger, G., Marschner, B., Flessa, H., 2006. Stabilization of organic matter in temperate soils: mechanisms and their relevance under different soil conditions – a review. European Journal of Soil Science 57, 426–445. https://doi.org/10.1111/j.1365-2389.2006.00809.x

Lynch, J.A., Clark, J.S., Bigelow, N.H., Edwards, M.E., Finney, B.P., 2002. Geographic and temporal variations in fire history in boreal ecosystems of Alaska. Journal of Geophysical Research 108. https://doi.org/10.1029/2001JD000332

MacDonald, G.M., Larsen, C.P.S., Szeicz, J.M., Moser, K.A., 1991. The reconstruction of boreal forest fire history from lake sediments: A comparison of charcoal, pollen, sedimentological, and geochemical indices. Quaternary Science Reviews 10, 53–71. https://doi.org/10.1016/0277-3791(91)90030-X

Marlon, J.R., Bartlein, P.J., Carcaillet, C., Gavin, D.G., Harrison, S.P., Higuera, P.E., Joos, F., Power, M.J., Prentice, I.C., 2008. Climate and human influences on global biomass burning over the past two millennia. Nature Geoscience 1, 697–702. https://doi.org/10.1038/ngeo313

Marlon, J.R., Bartlein, P.J., Daniau, A.-L., Harrison, S.P., Maezumi, S.Y., Power, M.J., Tinner, W., Vanniére, B., 2013. Global biomass burning: a synthesis and review of Holocene paleofire records and their controls. Quaternary Science Reviews 65, 5–25. https://doi.org/10.1016/j.quascirev.2012.11.029

Marlon, J.R., Bartlein, P.J., Gavin, D.G., Long, C.J., Anderson, R.S., Briles, C.E., Brown, K.J., Colombaroli, D., Hallett, D.J., Power, M.J., Scharf, E.A., Walsh, M.K., 2012. Long-term perspective on wildfires in the western USA. Proceedings of the National Academy of Sciences 109, E535–E543. https://doi.org/10.1073/pnas.1112839109

Masiello, C.A., 2004. New directions in black carbon organic geochemistry. Marine Chemistry 92, 201–213. https://doi.org/10.1016/j.marchem.2004.06.043

Masiello, C.A., Druffel, E.R.M., Currie, L.A., 2002. Radiocarbon measurements of black carbon in aerosols and ocean sediments. Geochimica et Cosmochimica Acta 66, 1025–1036. https://doi.org/10.1016/S0016-7037(01)00831-6

Miller, D.R., Castañeda, I.S., Bradley, R.S., MacDonald, D., 2017. Local and regional wildfire activity in central Maine (USA) during the past 900 years. J Paleolimnol 58, 455–466. https://doi.org/10.1007/s10933-017-0002-z

Miyazaki, Y., Kondo, Y., Han, S., Koike, M., Kodama, D., Komazaki, Y., Tanimoto, H., Matsueda, H., 2007. Chemical characteristics of water-soluble organic carbon in the Asian outflow. Journal of Geophysical Research 112. https://doi.org/10.1029/2007JD009116

Nakai, Y., 2016MS, Variation of elemental carbon supply to the Lake Suigetsu during the last 15 kyr, Master Thesis, Graduate School of Environmental Science, Hokkaido University.

Nakagawa, T., Gotanda, K., Haraguchi, T., Danhara, T., Yonenobu, H., Brauer, A., Yokoyama, Y., Tada, R., Takemura, K., Staff, R.A., Payne, R., Bronk Ramsey, C., Bryant, C., Brock, F., Schlolaut, G., Marshall, M., Tarasov, P., Lamb, H., 2012. SG06, a fully continuous and varved sediment core from Lake Suigetsu, Japan: stratigraphy and potential for improving the radiocarbon calibration model and understanding of late Quaternary climate changes. Quaternary Science Reviews 36, 164–176. https://doi.org/10.1016/j.quascirev.2010.12.013

Novakov, T., 1984. The role of soot and primary oxidants in atmospheric chemistry. Science of The Total Environment 36, 1–10. https://doi.org/10.1016/0048-9697(84)90241-9

Ohlson, M., Tryterud, E., 2000. Interpretation of the charcoal record in forest soils: forest fires and their production and deposition of macroscopic charcoal. The Holocene 10, 519–525. https://doi.org/10.1191/095968300667442551

Oris, F., Ali, A.A., Asselin, H., Paradis, L., Bergeron, Y., Finsinger, W., 2014. Charcoal dispersion and deposition in boreal lakes from 3 years of monitoring: Differences between local and regional fires. Geophysical Research Letters 41, 6743–6752. https://doi.org/10.1002/2014GL060984

Oshima, N., Kondo, Y., Moteki, N., Takegawa, N., Koike, M., Kita, K., Matsui, H., Kajino, M., Nakamura, H., Jung, J.S., Kim, Y.J., 2012. Wet removal of black carbon in Asian outflow: Aerosol Radiative Forcing in East Asia (A-FORCE)

aircraft campaign: Removal of black carbon. Journal of Geophysical Research: Atmospheres 117, n/a-n/a. https://doi.org/10.1029/2011JD016552

Peters, M.E., Higuera, P.E., 2007. Quantifying the source area of macroscopic charcoal with a particle dispersal model. Quaternary Research 67, 304–310. https://doi.org/10.1016/j.yqres.2006.10.004

Pokras, E.M., Mix, A.C., 1987. Earth's precession cycle and Quaternary climatic change in tropical Africa. Nature 326, 486–487. https://doi.org/10.1038/326486a0

Preston, C.M., Schmidt, M.W.I., 2006. Black (pyrogenic) carbon: a synthesis of current knowledge and uncertainties with special consideration of boreal regions. Biogeosciences 3, 397–420. https://doi.org/10.5194/bg-3-397-2006

Sah, J.P., Ross, M.S., Snyder, J.R., Koptur, S., Cooley, H.C., 2006. Fuel loads, fire regimes, and post-fire fuel dynamics in Florida Keys pine forests. International Journal of Wildland Fire 15, 16. https://doi.org/10.1071/WF05100

Santín, C., Doerr, S.H., Kane, E.S., Masiello, C.A., Ohlson, M., de la Rosa, J.M., Preston, C.M., Dittmar, T., 2016. Towards a global assessment of pyrogenic carbon from vegetation fires. Global Change Biology 22, 76–91. https://doi.org/10.1111/gcb.12985

Sato, M., Hansen, J., Koch, D., Lacis, A., Ruedy, R., Dubovik, O., Holben, B., Chin, M., Novakov, T., 2003. Global atmospheric black carbon inferred from AERONET. PNAS 100, 6319–6324. https://doi.org/10.1073/pnas.0731897100

Schlolaut, G., Brauer, A., Marshall, M.H., Nakagawa, T., Staff, R.A., Bronk Ramsey, C., Lamb, H.F., Bryant, C.L., Naumann, R., Dulski, P., Brock, F., Yokoyama, Y., Tada, R., Haraguchi, T., 2014. Event layers in the Japanese Lake Suigetsu 'SG06' sediment core: description, interpretation and climatic implications. Quaternary Science Reviews 83, 157–170. https://doi.org/10.1016/j.quascirev.2013.10.026

Schmidt, M.W.I., Skjemstad, J.O., Jäger, C., 2002. Carbon isotope geochemistry and nanomorphology of soil black carbon: Black chernozemic soils in central Europe originate from ancient biomass burning. Global Biogeochemical Cycles 16, 70-1-70–8. https://doi.org/10.1029/2002GB001939

Schneider, M.P.W., n.d. Assessment of a Molecular Marker Method to Determine the Pyrogenic Carbon Component in Charcoals and Soils 78.

Schneider, M.P.W., Hilf, M., Vogt, U.F., Schmidt, M.W.I., 2010. The benzene polycarboxylic acid (BPCA) pattern of wood pyrolyzed between 200°C and 1000°C. Organic Geochemistry 41, 1082–1088. https://doi.org/10.1016/j.orggeochem.2010.07.001

Schneider, M.P.W., Lehmann, J., Schmidt, M.W.I., 2011a. Charcoal quality does not change over a century in a tropical agro-ecosystem. Soil Biology and Biochemistry 43, 1992–1994. https://doi.org/10.1016/j.soilbio.2011.05.020

Schneider, M.P.W., Pyle, L.A., Clark, K.L., Hockaday, W.C., Masiello, C.A., Schmidt, M.W.I., 2013. Toward a "Molecular Thermometer" to Estimate the Charring Temperature of Wildland Charcoals Derived from Different Biomass Sources. Environmental Science & Technology 47, 11490–11495.

https://doi.org/10.1021/es401430f
Schneider, M.P.W., Smittenberg, R.H., Dittmar, T., Schmidt, M.W.I., 2011b. Comparison of gas with liquid chromatography for the determination of benzenepolycarboxylic acids as molecular tracers of black carbon. Organic Geochemistry 42, 275–282. https://doi.org/10.1016/j.orggeochem.2011.01.003
Scott, A.C., 2010. Charcoal recognition, taphonomy and uses in palaeoenvironmental analysis. Palaeogeography, Palaeoclimatology, Palaeoecology 291, 11–39. https://doi.org/10.1016/j.palaeo.2009.12.012
Scott, A.C., 2000. The Pre-Quaternary history of fire. Palaeogeography, Palaeoclimatology, Palaeoecology 164, 281–329. https://doi.org/10.1016/S0031-0182(00)00192-9
Seiler, W., Crutzen, P.J., 1980. Estimates of gross and net fluxes of carbon between the biosphere and the atmosphere from biomass burning. Climatic Change 2, 207–247. https://doi.org/10.1007/BF00137988
Singh, N., Abiven, S., Maestrini, B., Bird, J.A., Torn, M.S., Schmidt, M.W.I., 2014. Transformation and stabilization of pyrogenic organic matter in a temperate forest field experiment. Global Change Biology 20, 1629–1642. https://doi.org/10.1111/gcb.12459
Site U1423, 2015. , Proceedings of the IODP. Integrated Ocean Drilling Program. https://doi.org/10.2204/iodp.proc.346.2015
Stewart, C.E., Zheng, J., Botte, J., Cotrufo, M.F., 2013. Co-generated fast pyrolysis biochar mitigates green-house gas emissions and increases carbon sequestration in temperate soils. GCB Bioenergy 5, 153–164. https://doi.org/10.1111/gcbb.12001
Sun, X., Luo, Y., Huang, F., Tian, J., Wang, P., 2003. Deep-sea pollen from the South China Sea: Pleistocene indicators of East Asian monsoon. Marine Geology 201, 97–118. https://doi.org/10.1016/S0025-3227(03)00211-1
Sun, Y., Chen, J., Clemens, S.C., Liu, Q., Ji, J., Tada, R., 2006. East Asian monsoon variability over the last seven glacial cycles recorded by a loess sequence from the northwestern Chinese Loess Plateau. Geochemistry, Geophysics, Geosystems 7, 1–16. https://doi.org/10.1029/2006GC001287
Suzuki, Y., Tada, R., Yamada, K., Irino, T., Nagashima, K., Nakagawa, T., Omori, T., 2016. Mass accumulation rate of detrital materials in Lake Suigetsu as a potential proxy for heavy precipitation: a comparison of the observational precipitation and sedimentary record. Progress in Earth and Planetary Science 3, 5. https://doi.org/10.1186/s40645-016-0081-x
Swift, R.S., 2001. SEQUESTRATION OF CARBON BY SOIL: Soil Science 166, 858–871. https://doi.org/10.1097/00010694-200111000-00010
Tada, R., Irino, T., Ikehara, K., Karasuda, A., Sugisaki, S., Xuan, C., Sagawa, T., Itaki, T., Kubota, Y., Lu, S., Seki, A., Murray, R.W., Alvarez-Zarikian, C., Anderson, W.T., Bassetti, M.-A., Brace, B.J., Clemens, S.C., da Costa Gurgel, M.H., Dickens, G.R., Dunlea, A.G., Gallagher, S.J., Giosan, L., Henderson, A.C.G., Holbourn, A.E., Kinsley, C.W., Lee, G.S., Lee, K.E., Lofi, J., Lopes, C.I.C.D., Saavedra-Pellitero, M., Peterson, L.C., Singh, R.K., Toucanne, S., Wan, S.,

Zheng, H., Ziegler, M., 2018. High-resolution and high-precision correlation of dark and light layers in the Quaternary hemipelagic sediments of the Japan Sea recovered during IODP Expedition 346. Progress in Earth and Planetary Science 5. https://doi.org/10.1186/s40645-018-0167-8

Tada, R., Irino, T., Koizumi, I., 1999. Land-ocean linkages over orbital and millennial timescales recorded in Late Quaternary sediments of the Japan Sea. Paleoceanography 14, 236–247. https://doi.org/10.1029/1998PA900016

Théry-Parisot, I., Chabal, L., Chrzavzez, J., 2010. Anthracology and taphonomy, from wood gathering to charcoal analysis. A review of the taphonomic processes modifying charcoal assemblages, in archaeological contexts. Palaeogeography, Palaeoclimatology, Palaeoecology 291, 142–153. https://doi.org/10.1016/j.palaeo.2009.09.016

Thevenon, F., Williamson, D., Bard, E., Anselmetti, F.S., Beaufort, L., Cachier, H., 2010. Combining charcoal and elemental black carbon analysis in sedimentary archives: Implications for past fire regimes, the pyrogenic carbon cycle, and the human–climate interactions. Global and Planetary Change 72, 381–389. https://doi.org/10.1016/j.gloplacha.2010.01.014

Tinner, W., Hofstetter, S., Zeugin, F., Conedera, M., Wohlgemuth, T., Zimmermann, L., Zweifel, R., 2006. Long-distance transport of macroscopic charcoal by an intensive crown fire in the Swiss Alps - implications for fire history reconstruction. The Holocene 16, 287–292. https://doi.org/10.1191/0959683606hl925rr

Urabe, T., Kuriyama, M., Matsumoto, R., Kumon, F., 2014. Late Quaternary climates of East Asia deduced from the total organic carbon contents of cored sediments (MD179-3304, 3312) off Joetsu City, Japan Sea. Journal of Asian Earth Sciences 90, 209–217. https://doi.org/10.1016/j.jseaes.2013.07.036

Vachula, R.S., Richter, N., 2018. Informing sedimentary charcoal-based fire reconstructions with a kinematic transport model. The Holocene 28, 173–178. https://doi.org/10.1177/0959683617715624

Vachula, R.S., Russell, J.M., Huang, Y., Richter, N., 2018a. Assessing the spatial fidelity of sedimentary charcoal size fractions as fire history proxies with a high-resolution sediment record and historical data. Palaeogeography, Palaeoclimatology, Palaeoecology 508, 166–175. https://doi.org/10.1016/j.palaeo.2018.07.032

Vachula, R.S., Santos, E., Alexandre, M.R., Huang, Y., 2018b. Comparison of black carbon chemical oxidation and macroscopic charcoal counts for quantification of fire by-products in sediments. Organic Geochemistry 125, 50–54. https://doi.org/10.1016/j.orggeochem.2018.08.011

Verardo, D.J., Ruddiman, W.F., 1996. Late Pleistocene charcoal in tropical Atlantic deep-sea sediments: climate and geochemical significance. Geology 24, 855–857. https://doi.org/10.1130/0091-7613(1996)024<0855

WANG, P., 2003. Evolution of the South China Sea and monsoon history revealed in deep-sea records. Chinese Science Bulletin 48, 2549. https://doi.org/10.1360/03wd0156

Whitlock, C., Millspaugh, S.H., 1996. Testing the assumptions of fire-history studies: an examination of modern charcoal accumulation in Yellowstone National Park, USA. The Holocene 6, 7–15. https://doi.org/10.1177/095968369600600102

Wiedemeier, D.B., Abiven, S., Hockaday, W.C., Keiluweit, M., Kleber, M., Masiello, C.A., McBeath, A.V., Nico, P.S., Pyle, L.A., Schneider, M.P.W., Smernik, R.J., Wiesenberg, G.L.B., Schmidt, M.W.I., 2015. Aromaticity and degree of aromatic condensation of char. Organic Geochemistry 78, 135–143. https://doi.org/10.1016/j.orggeochem.2014.10.002

Wiedemeier, D.B., Lang, S.Q., Gierga, M., Abiven, S., Bernasconi, S.M., Früh-Green, G.L., Hajdas, I., Hanke, U.M., Hilf, M.D., McIntyre, C.P., Scheider, M.P.W., Smittenberg, R.H., Wacker, L., Wiesenberg, G.L.B., Schmidt, M.W.I., 2016. Characterization, Quantification and Compound-specific Isotopic Analysis of Pyrogenic Carbon Using Benzene Polycarboxylic Acids (BPCA). JoVE (Journal of Visualized Experiments) e53922–e53922. https://doi.org/10.3791/53922

Wiedner, K., Naisse, C., Rumpel, C., Pozzi, A., Wieczorek, P., Glaser, B., 2013. Chemical modification of biomass residues during hydrothermal carbonization – What makes the difference, temperature or feedstock? Organic Geochemistry 54, 91–100. https://doi.org/10.1016/j.orggeochem.2012.10.006

Wolf, M., Lehndorff, E., Mrowald, M., Eckmeier, E., Kehl, M., Frechen, M., Pätzold, S., Amelung, W., 2014. Black carbon: Fire fingerprints in Pleistocene loess–palaeosol archives in Germany. Organic Geochemistry 70, 44–52. https://doi.org/10.1016/j.orggeochem.2014.03.002

Wolf, M., Lehndorff, E., Wiesenberg, G.L.B., Stockhausen, M., Schwark, L., Amelung, W., 2013. Towards reconstruction of past fire regimes from geochemical analysis of charcoal. Organic Geochemistry 55, 11–21. https://doi.org/10.1016/j.orggeochem.2012.11.002

Xiao, J.L., An, Z.S., Liu, T.S., Inouchi, Y., Kumai, H., Yoshikawa, S., Kondo, Y., 1999. East Asian monsoon variation during the last 130,000 Years: evidence from the Loess Plateau of central China and Lake Biwa of Japan. Quaternary Science Reviews 18, 147–157. https://doi.org/10.1016/S0277-3791(97)00097-8

Yarnes, C., Santos, F., Singh, N., Abiven, S., Schmidt, M.W.I., Bird, J.A., n.d. Stable isotopic analysis of pyrogenic organic matter in soils by liquid chromatography–isotope-ratio mass spectrometry of benzene polycarboxylic acids. Rapid Communications in Mass Spectrometry 25, 3723–3731. https://doi.org/10.1002/rcm.5272

Yoon, J.-H., Kawamura, H., 2002. The Formation and Circulation of the Intermediate Water in the Japan Sea. Journal of Oceanography 58, 197–211. https://doi.org/10.1023/A:1015893104998

Yoon, J.-H., Kim, Y.-J., 2009. Review on the seasonal variation of the surface circulation in the Japan/East Sea. Journal of Marine Systems 78, 226–236. https://doi.org/10.1016/j.jmarsys.2009.03.003

Zhang, Z., Xing, W., Wang, G., Tong, S., Lv, X., Sun, J., 2015a. The peatlands developing history in the Sanjiang Plain, NE China and its response to East

Asian monsoon variation. Scientific Reports 5. https://doi.org/10.1038/srep11316

Zhang, Z., Zhong, J., Lv, X., Tong, S., Wang, G., 2015b. Climate, vegetation, and human influences on late-Holocene fire regimes in the Sanjiang plain, northeastern China. Palaeogeography, Palaeoclimatology, Palaeoecology 438, 1–8. https://doi.org/10.1016/j.palaeo.2015.07.028

Zhou, B., Shen, C., Sun, W., Zheng, H., Yang, Y., Sun, Y., An, Z., 2007. Elemental carbon record of paleofire history on the Chinese Loess Plateau during the last 420 ka and its response to environmental and climate changes. Palaeogeography, Palaeoclimatology, Palaeoecology 252, 617–625. https://doi.org/10.1016/j.palaeo.2007.05.014

Zimmerman, A.R., 2010. Abiotic and Microbial Oxidation of Laboratory-Produced Black Carbon (Biochar). Environ. Sci. Technol. 44, 1295–1301. https://doi.org/10.1021/es903140c

Zimmerman, A.R., Gao, B., 2013. The Stability of Biochar in the Environment [WWW Document]. Biochar and Soil Biota. https://doi.org/10.1201/b14585-3

Figure captions

Figure 1 The black carbon combustion continuum.

Figure 2 BC transportation from fire center to sediment. The samples of Atmospheric sediment traps, Lake sediment traps, Lake sediment cores, Lake sediment cores (tree ring comparison) and Lake surface sediment are shown as black dots, black triangle, green triangle, red dots and blue triangle.

Figure 3 Map showing the studied sea area and location of Site U1423. The locations of ① Site 795, ② Site 794, and ③ Site 797 in Heusser (1992) and ④ Site GH02–1030 in Igarashi et al. (2011) are also shown (from Igarashi et al., 2018).

Figure 4 Revised age model for U1423 based on projection of the "U1424_LR04 tuned age" (Tada et al., 2018) to Site U1423 by the inter-site correlation of dark-light cycles for the last 1.5 Ma (red inverted triangles) and tuning of the GRA profile to the LR04 stack (vertical lines). Assuming that a high GRA represents glacial maxima, 118 horizons have been correlated to maxima of the oxygen isotope profile of LR04 for the last 2.975 Myr (Lu et al., 2018).

Figure 5 The age-depth relationship of the revised age model for Site U1423 used in this study (Lu et al., 2018). The age control points from the Expedition Report (Tada et

al., 2015) is also indicated by the black dots and lines.

Figure 6 Map showing the observation sites of KR15-10. The locations of Site WB6, Site WB8 are also shown.

Figure 7 Location of Lake Suigetsu (modified after Nakagawa et al. 2005). Also shown are the location of core SG12LM3 and other coring sites (shown as numbers)(Suzuki et al., 2016).

Figure 8 The age-depth relationship of the revised age model for the core SG12LM3 used in this study (Suzuki et al., 2016).

Figure 9 The analytical scheme diagram for thermal optical transmittance (TOT) method.

Figure 10 The device schematic of thermal optical transmittance (TOT).

Figure 11 (a) An example thermal optical transmittance (TOT) thermogram (Lu et al., 2018). Temperature change is represented as red line, and the corrected laser transmission ratio is represented by orange line. The carbon fraction detected by NDIR response is represented as black line. (b) The relationship between the ambient temperature and the original laser transmission generated by a Semi-Continuous OCEC

Carbon Aerosol Analyser manufactured by Sunset Laboratory. The temperature dependency of the raw laser transmission values was calibrated using a quadratic relationship, with the ambient temperatures shown as red dots (Lu et al., 2018).

Figure 12 The analytical scheme diagram for benzene polycarboxylic acids (BPCA) method.

Figure 13 Yields of B3CA (sum), B4CA, B5CA and B6CA from wood (first line) and leaves (second line) charcoal with pyrolysis temperatures at 350 °C, 550 °C, and 850 °C, normalized to BPCA content. The pyrolysis temperatures at 350 °C, 550 °C, and 850 °C are shown as silver gray, tin gray and tungsten gray, respectively.

Figure 14 B6CA (%) in wood and leaves charcoal with pyrolysis temperature at 350 °C, 550 °C, and 850 °C. Treatment temperatures are shown as silver gray for 350 °C, tin gray for 550 °C , and tungsten gray for 850 °C.

Figure 15 B6CA (%) in European grass and wood charcoal with pyrolysis temperature at 200 ~ 1000 °C. Treatment temperatures are shown as tin gray for grass , and tungsten gray for wood.

Figure 16 Relationship between B6CA (%) and pyrolysis temperature for the total samples. The grey lines represent the 95% of confidence interval envelopes. The wood

and leaves charcoal (5 plants) are shown as black dots and gray inverted triangle, respectively.

Figure 17 Relationship between B6CA (%) and pyrolysis temperature for the European and East Asian samples. The European plants and East Asian plants charcoal are shown as black dots and red inverted triangle, respectively.

Figure 18 Relationship between BPCA sum and Total EC (include: Coarse EC, Fine EC) content for the total samples. The samples of Japan Sea U1423, Wakasa Bay KR15-10 Sites WB6 & 8 and Lake Suigetsu SG-12 are shown as black dots, blue dots, red dots and green dots, respectively.

Figure 19 Temporal variations in contents of B6CA, B5CA, B4CA, B3CA, BPCA sum, coarse EC, fine EC, total EC and the ratio of Fine EC / Coarse EC. The contents of B6CA, B5CA, B4CA, B3CA, coarse EC, fine EC are represented as red, blue , green, pink, black, orange color. The ratio of Fine EC / Coarse EC are shown as black line.

Figure 20 Temporal variations in B6CA (%), B5CA (%), B4CA (%) and B3CA (%). The B6CA (%), B5CA (%), B4CA (%) and B3CA (%) are represented as red, blue , green and pink color.

Figure 21 Temporal variations in contents of B6CA, B5CA, B4CA, B3CA, BPCA sum,

coarse EC, fine EC, total EC, the ratio of Fine EC / Coarse EC and B6CA (%). The contents of B6CA, B5CA, B4CA, B3CA, coarse EC, fine EC are represented as red, blue , green, pink, black, orange color. The ratio of Fine EC / Coarse EC are shown as black line. B6CA (%) are represented as gradient red color.

Figure 22 Temporal variations in contents of B6CA, B5CA, B4CA, B3CA, BPCA sum, coarse EC, fine EC, total EC and the ratio of Fine EC / Coarse EC. The contents of B6CA, B5CA, B4CA, B3CA, coarse EC, fine EC are represented as red, blue , green, pink, black, orange color. The ratio of Fine EC / Coarse EC are shown as black line.

Figure 23 Relationship between pollen content and EC content in the coarse fraction at Site U1423. The grey lines represent the 95% of confidence interval envelopes.

Figure 24 Relationship between Taxodiaceae and EC content in the coarse fraction at Site U1423.

Figure 25 LR04 standard benthic $\delta^{18}O$ (Lisiecki and Raymo, 2005) and pollen content. The significant maxima observed in the pollen content are marked as orange vertical lines corresponding to interglacial stages.

Figure 26 LR04 standard benthic $\delta^{18}O$ (Lisiecki and Raymo, 2005) and the fire temperature estimated from B6CA (%). The significant observed in the low and higher

temperature biomass burning are marked as pink and orange vertical lines corresponding to glacial and interglacial stages, respectively.

Figure 27 Temporal variations in contents of B6CA, B5CA, B4CA, B3CA, BPCA sum, coarse EC, fine EC, total EC and the ratio of Fine EC / Coarse EC. The contents of B6CA, B5CA, B4CA, B3CA, coarse EC, fine EC are represented as red, blue , green, pink, black, orange color. The ratio of Fine EC / Coarse EC are shown as black line.

Figure 28 Chinese Stalagmite $\delta^{18}O$ (Cheng et al., 2016) and the fire temperature estimated from B6CA (%). The significant observed in the low and higher temperature biomass burning are marked as pink and orange vertical lines corresponding to East Asian summer monsoon (EASM) weak and strong stages, respectively.

Table captions

Table 1. The plant species settings for this study.

Table 2. The control points for age model.

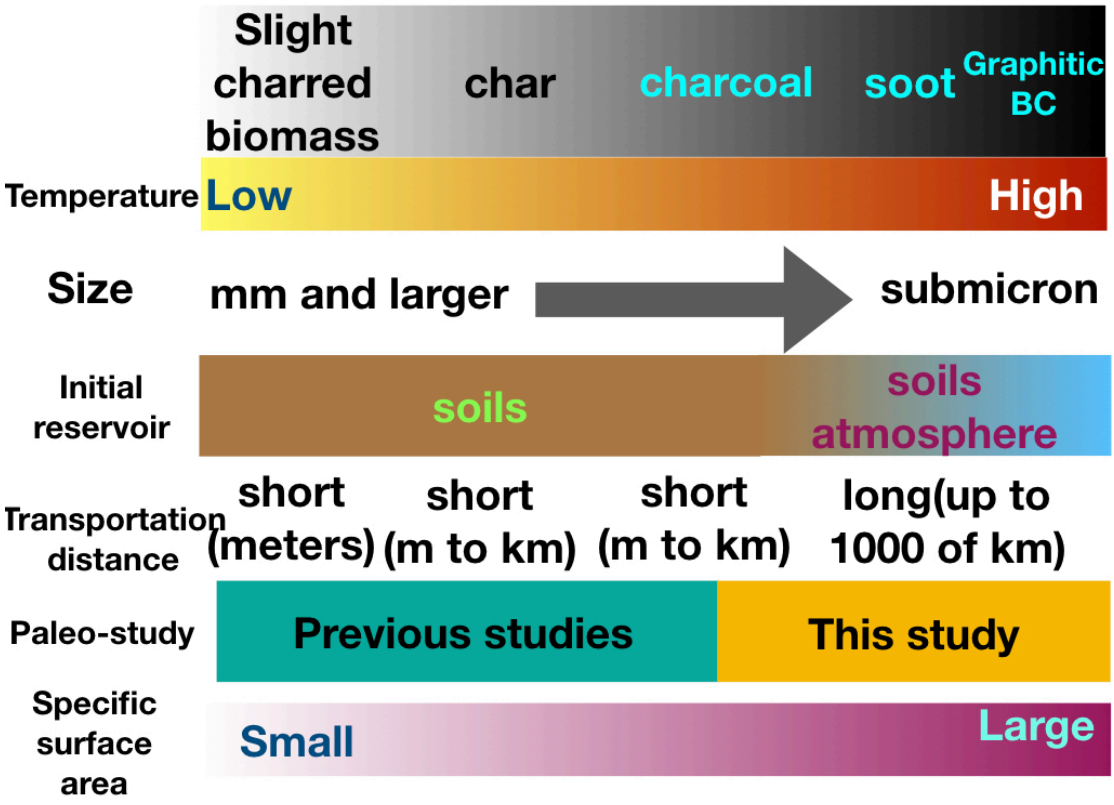

Figure 1. The black carbon combustion continuum.

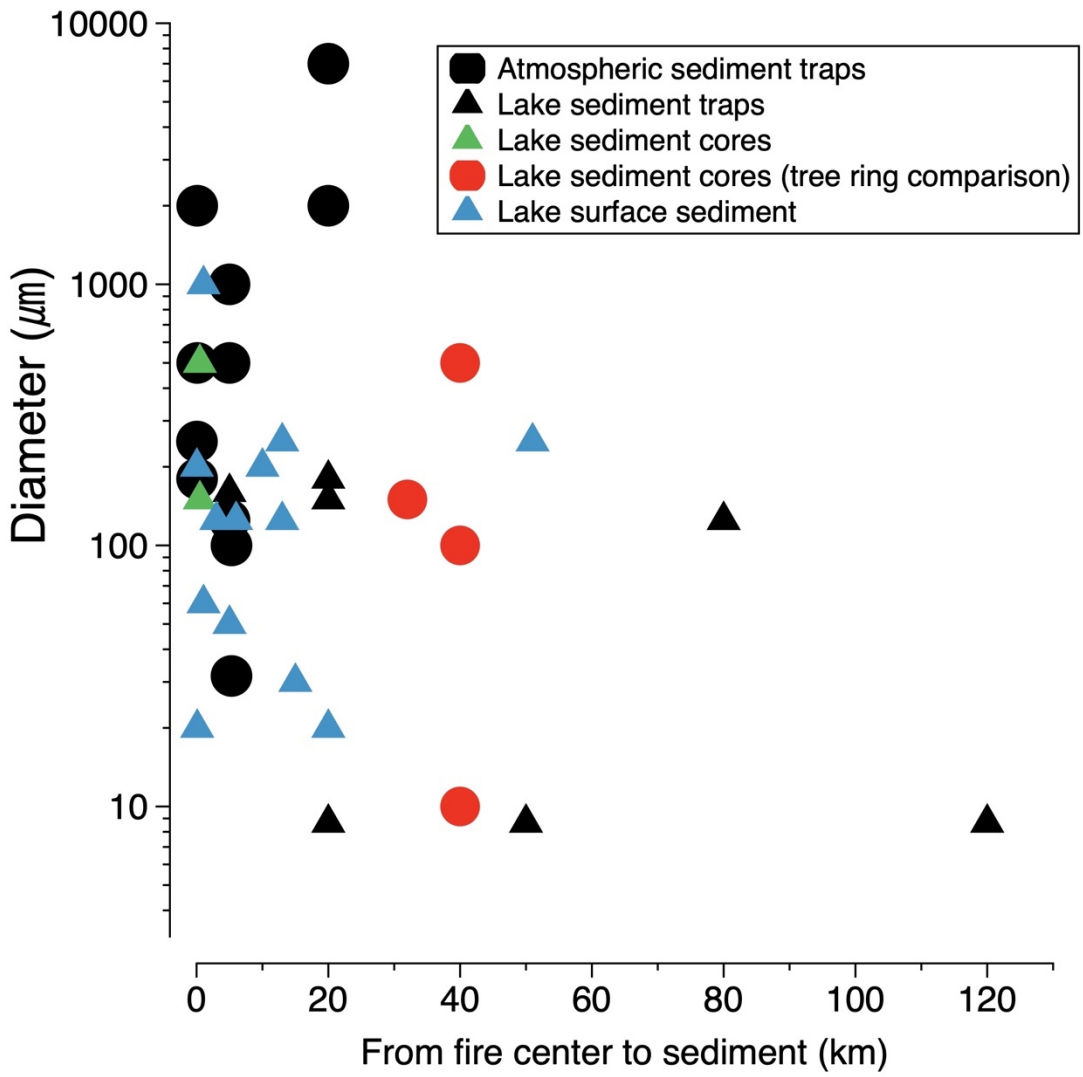

Figure 2. BC transportation from fire center to sediment. The samples of Atmospheric sediment traps, Lake sediment traps, Lake sediment cores, Lake sediment cores (tree ring comparison) and Lake surface sediment are shown as black dots, black triangle, green triangle, red dots and blue triangle.

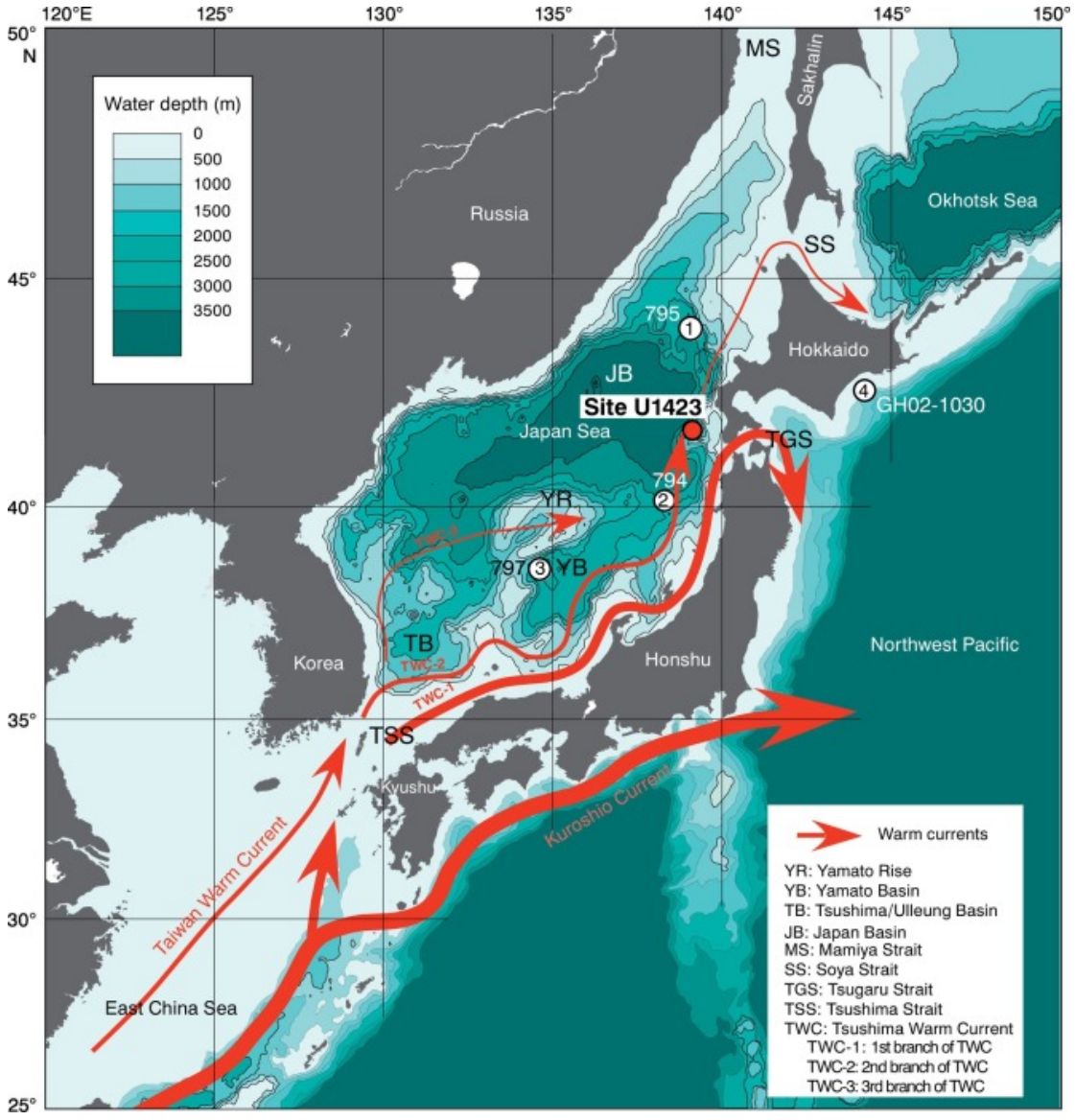

Figure 3. Map showing the studied sea area and location of Site U1423. The locations of ① Site 795, ② Site 794, and ③ Site 797 in Heusser (1992) and ④ Site GH02–1030 in Igarashi et al. (2011) are also shown (from Igarashi et al., 2018).

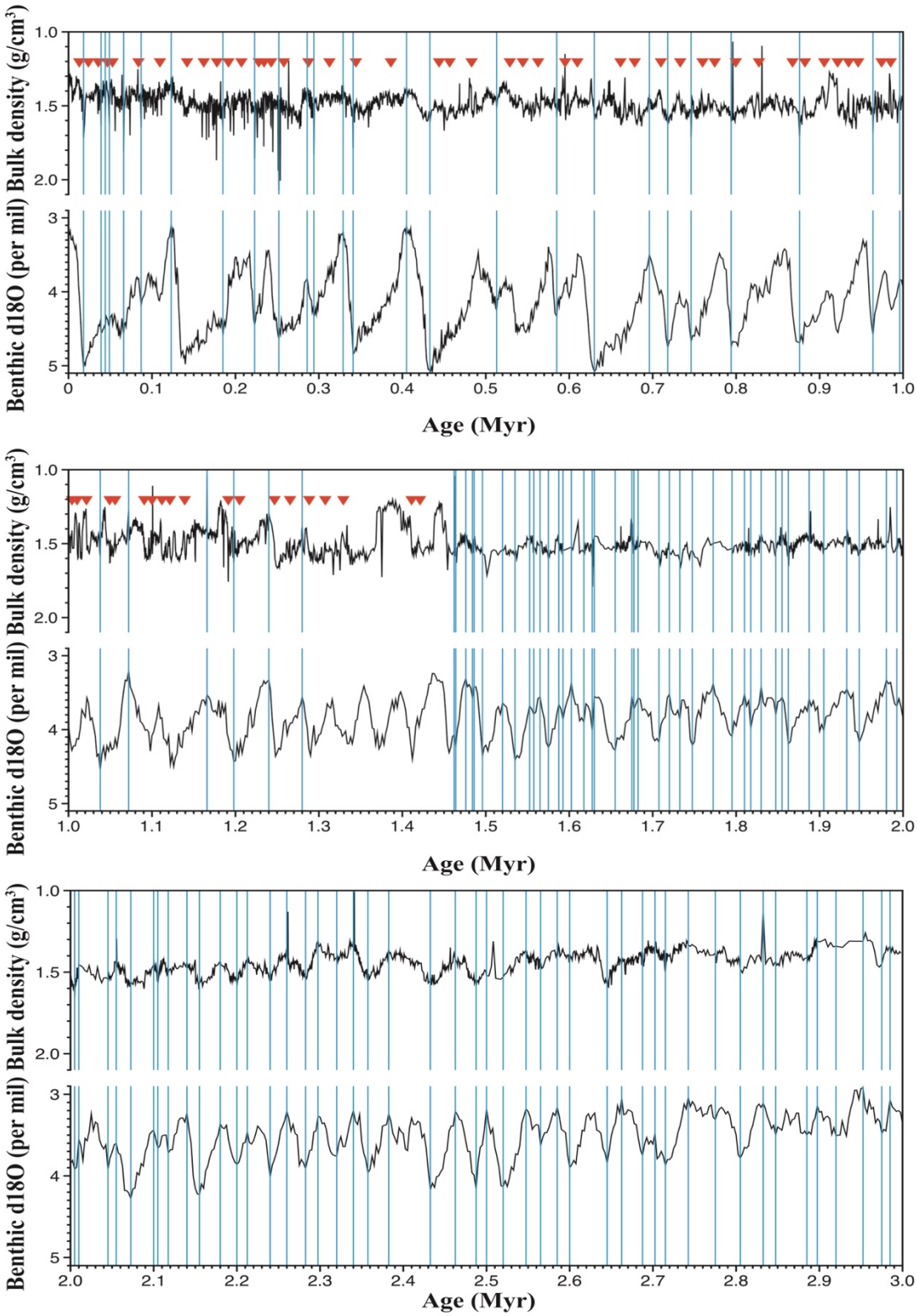

Figure 4. Revised age model for U1423 based on projection of the "U1424_LR04 tuned age" (Tada et al., 2018) to Site U1423 by the inter-site correlation of dark-light cycles for the last 1.5 Ma (red inverted triangles) and tuning of the GRA profile to the LR04 stack (vertical lines). Assuming that a high GRA represents glacial maxima, 118 horizons have been correlated to maxima of the oxygen isotope profile of LR04 for the last 2.975 Myr (Lu et al., 2018).

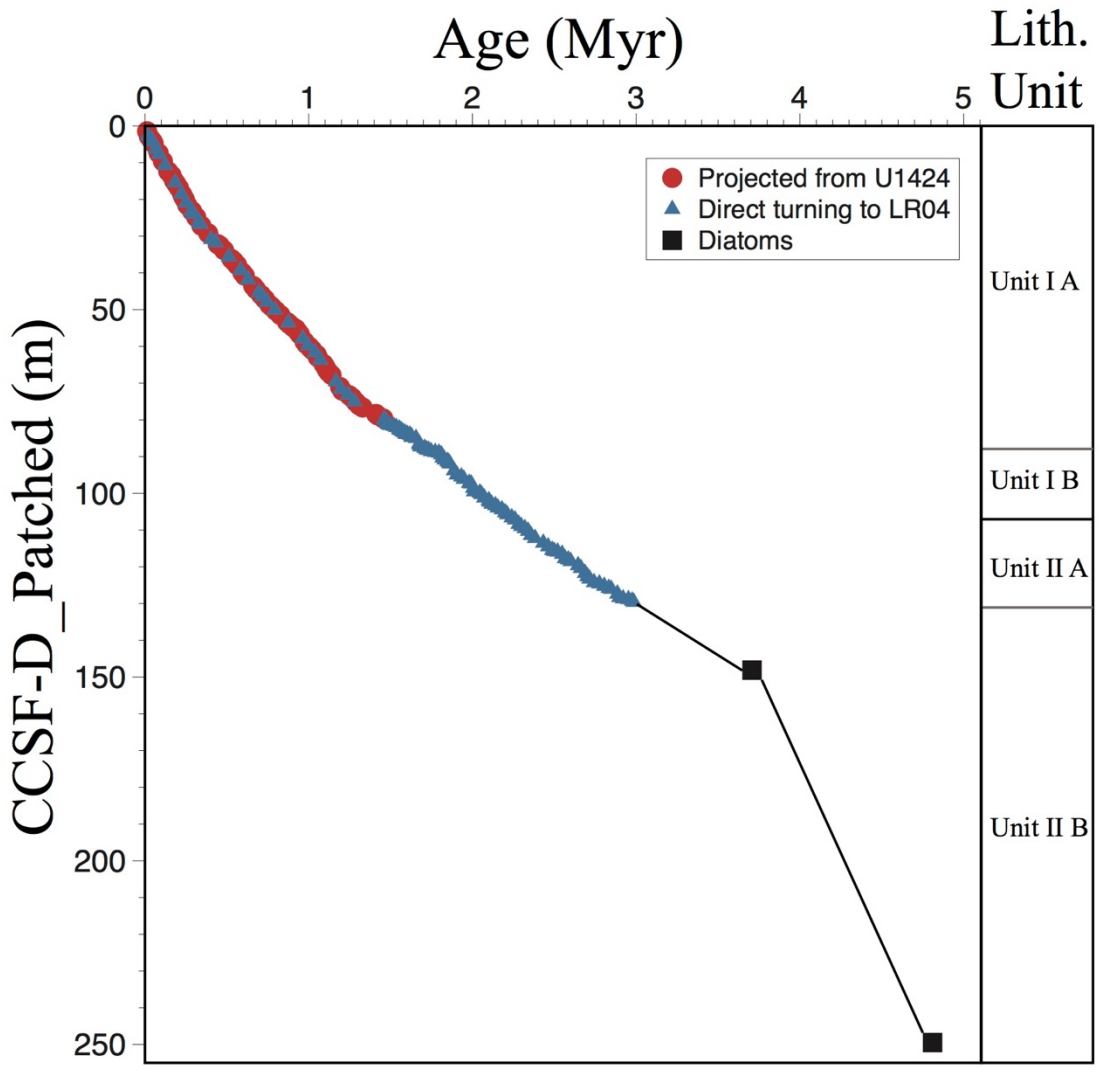

Figure 5. The age-depth relationship of the revised age model for Site U1423 used in this study (Lu et al., 2018). The age control points from the Expedition Report (Tada et al., 2015) is also indicated by the black dots and lines.

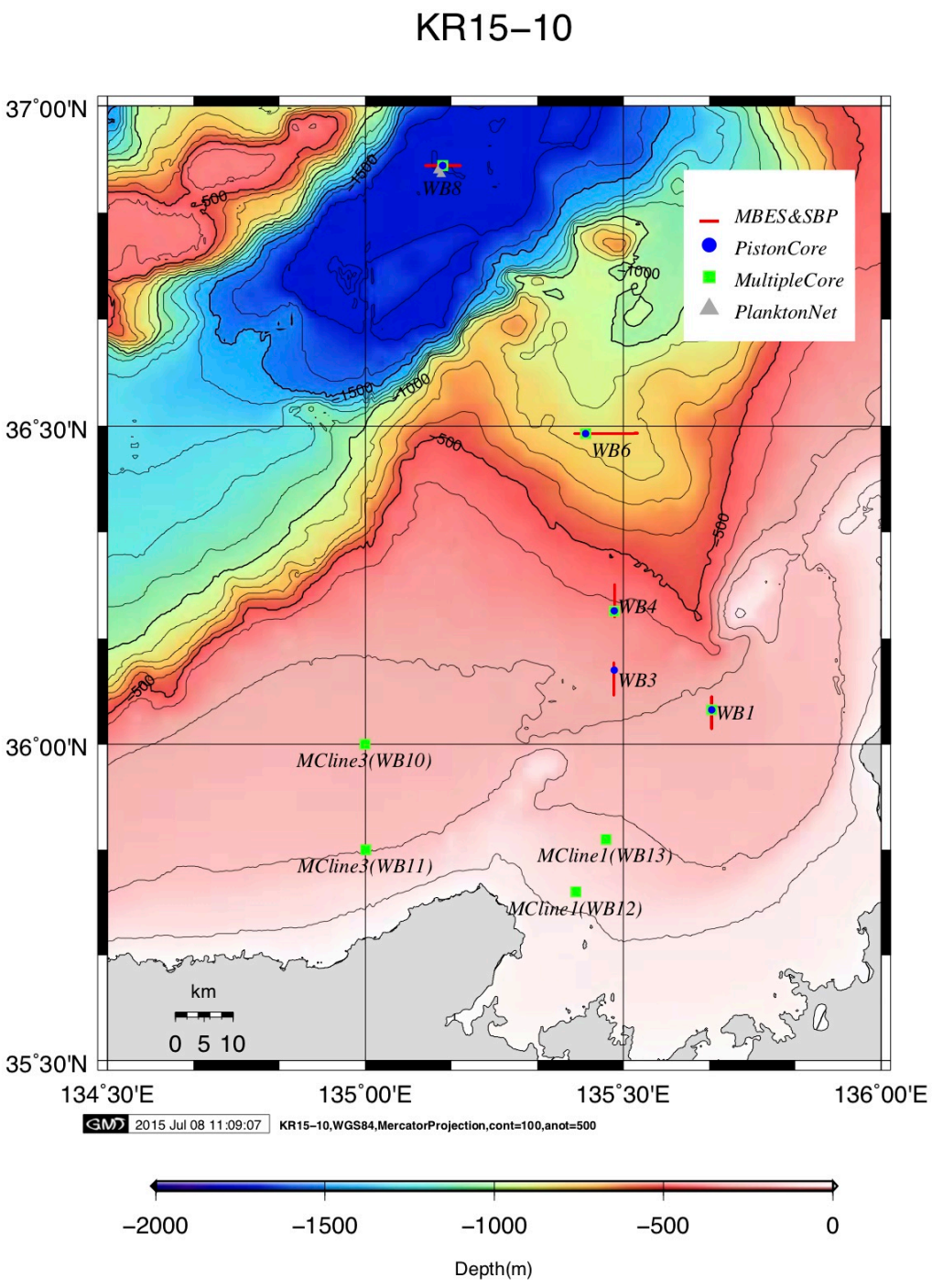

Figure 6. Map showing the observation sites of KR15-10. The locations of Site WB6, Site WB8 are also shown.

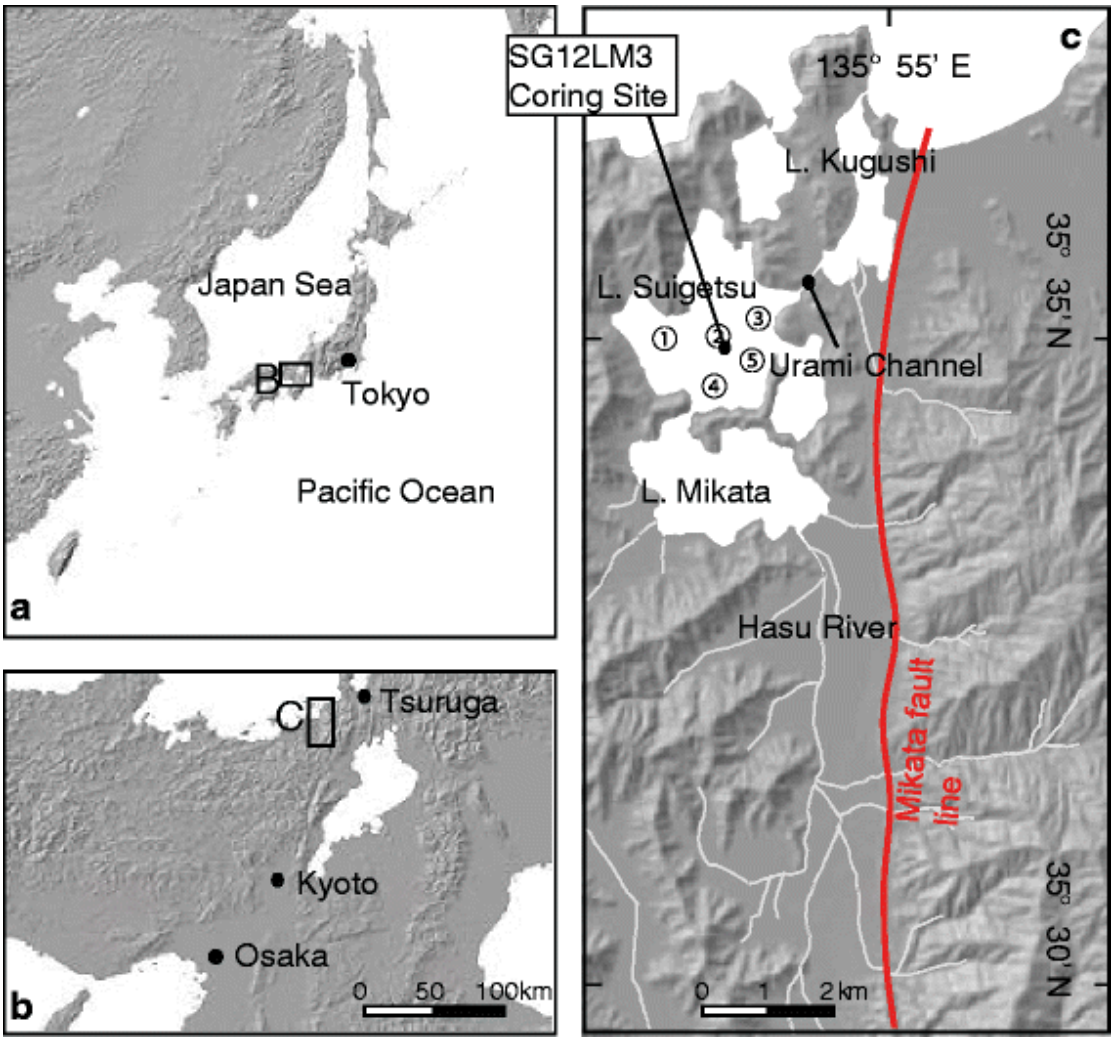

Figure 7. Location of Lake Suigetsu (modified after Nakagawa et al. 2005). Also shown are the location of core SG12LM3 and other coring sites (shown as numbers)(Suzuki et al., 2016).

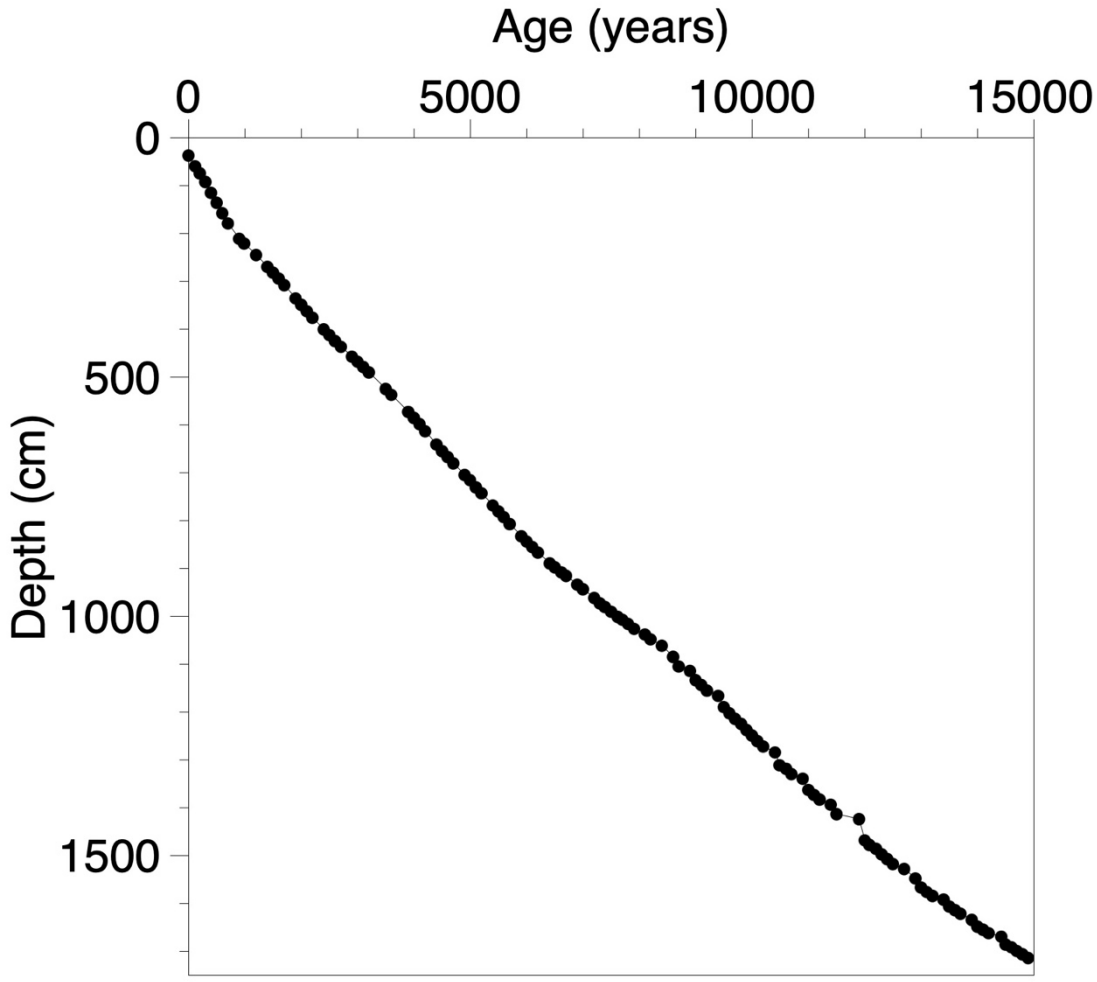

Figure 8. The age-depth relationship of the revised age model for the core SG12LM3 used in this study (Suzuki et al., 2016).

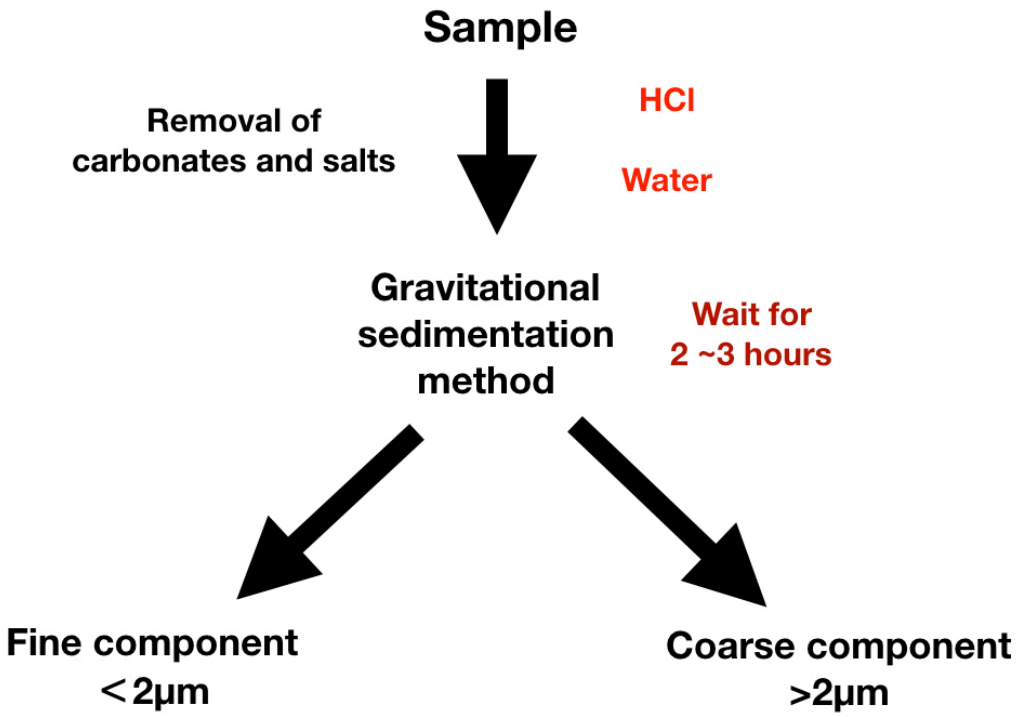

Figure 9. The analytical scheme diagram for thermal optical transmittance (TOT) method.

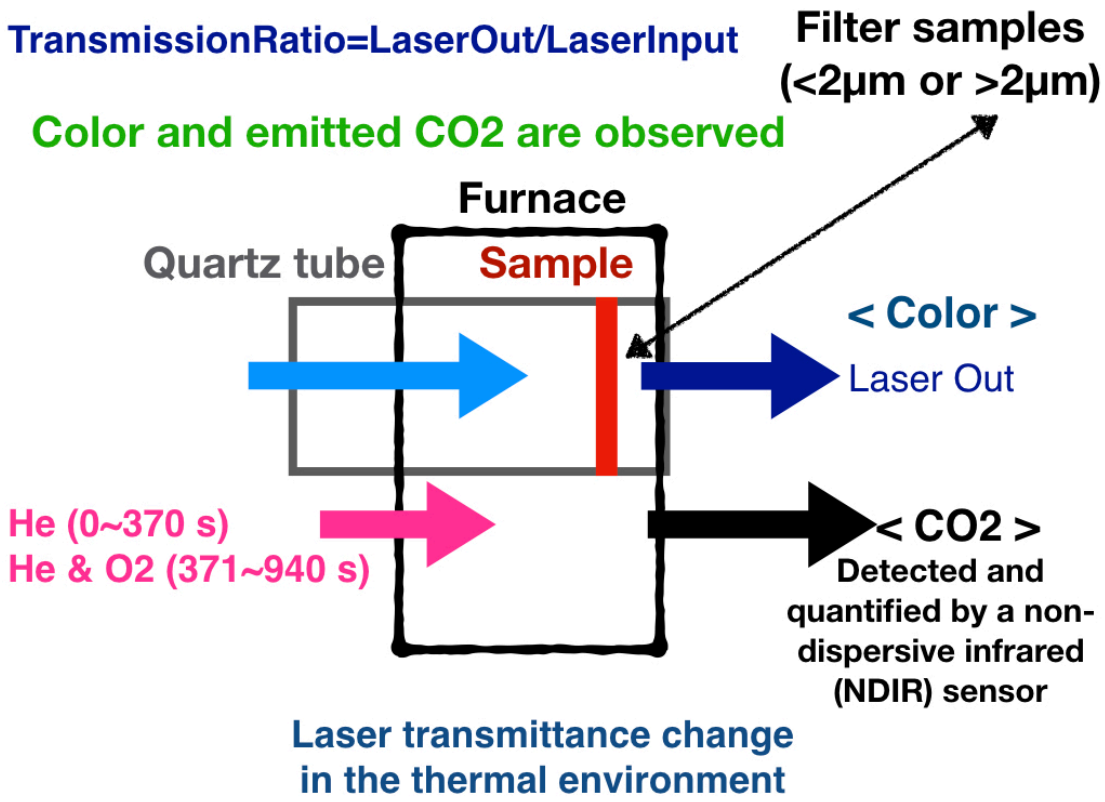

Figure 10. The device schematic of thermal optical transmittance (TOT).

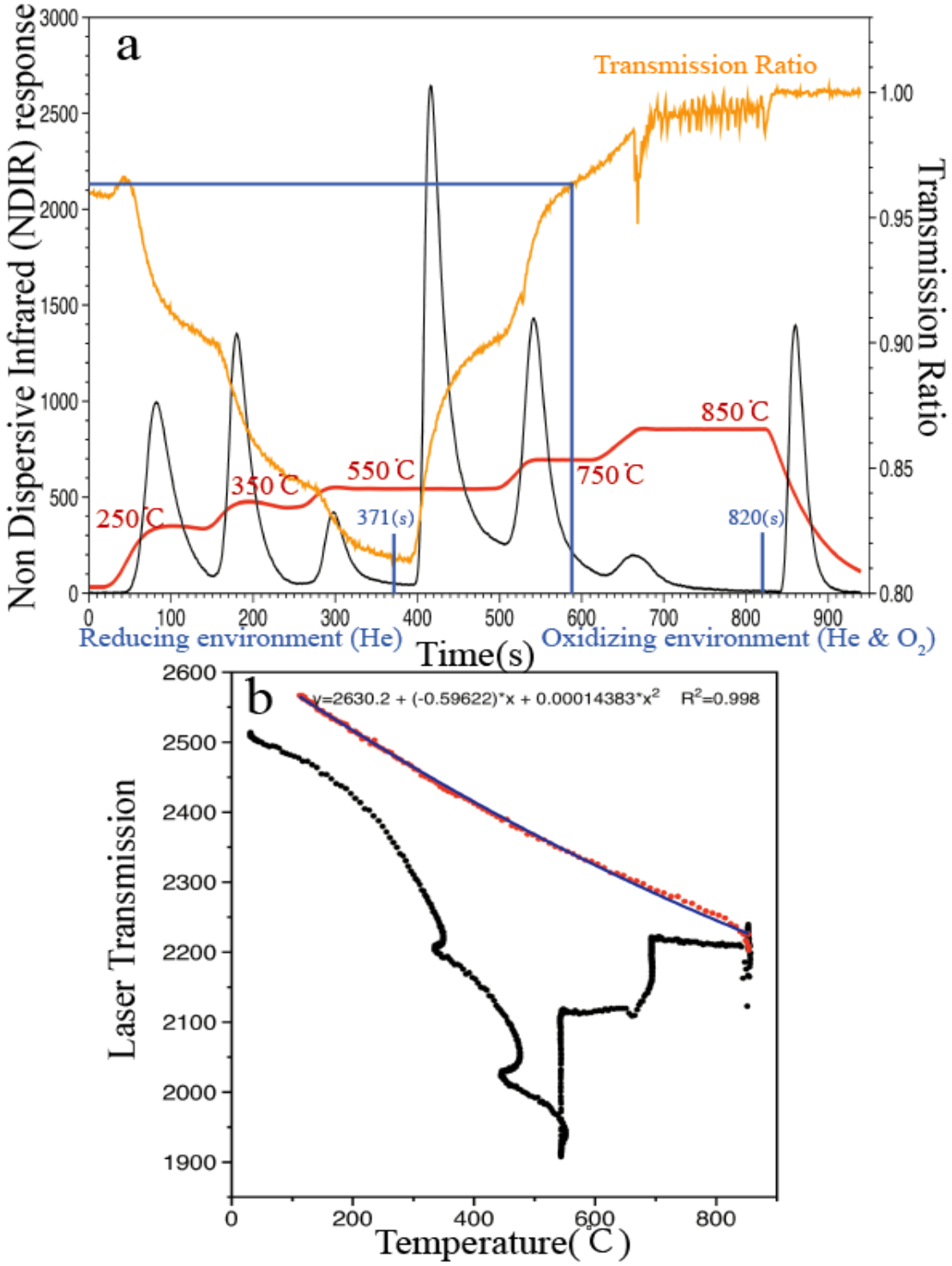

Figure 11. (a) An example thermal optical transmittance (TOT) thermogram (Lu et al., 2018). Temperature change is represented as red line, and the corrected laser transmission ratio is represented by orange line. The carbon fraction detected by NDIR response is represented as black line. (b) The relationship between the ambient temperature and the original laser transmission generated by a Semi-Continuous OCEC Carbon Aerosol Analyser manufactured by Sunset Laboratory. The temperature dependency of the raw laser transmission values was calibrated using a quadratic relationship, with the ambient temperatures shown as red dots (Lu et al., 2018).

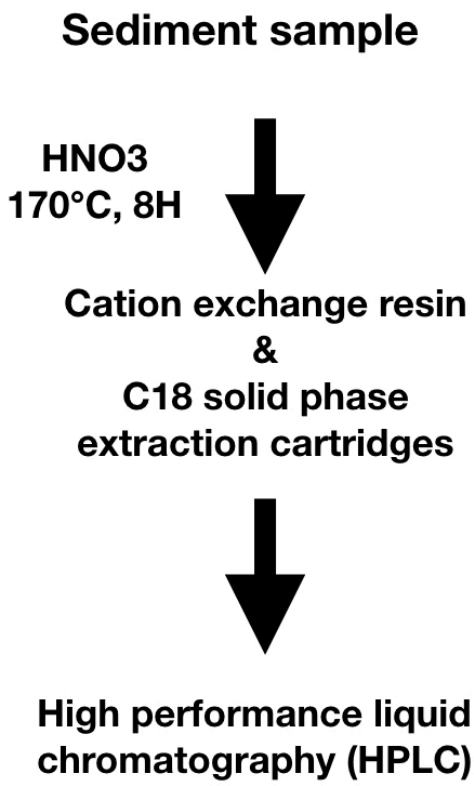

Figure 12. The analytical scheme diagram for benzene polycarboxylic acids (BPCA).

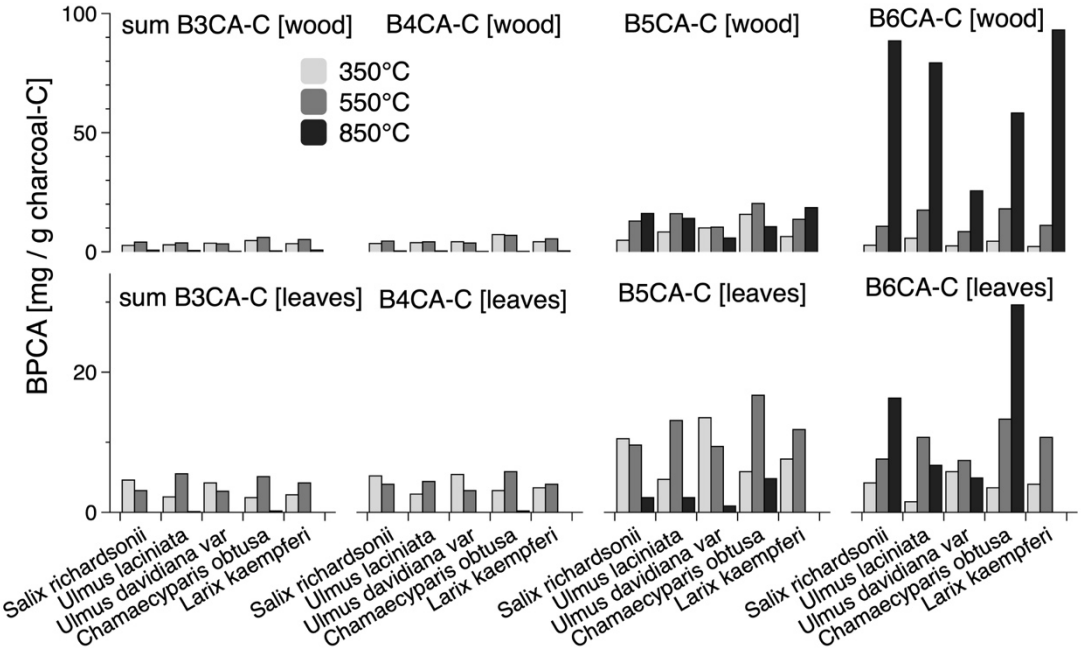

Figure 13. Yields of B3CA (sum), B4CA, B5CA and B6CA from wood (first line) and leaves (second line) charcoal with pyrolysis temperatures at 350 °C, 550 °C, and 850 °C, normalized to BPCA content. The pyrolysis temperatures at 350 °C, 550 °C, and 850 °C are shown as silver gray, tin gray and tungsten gray, respectively.

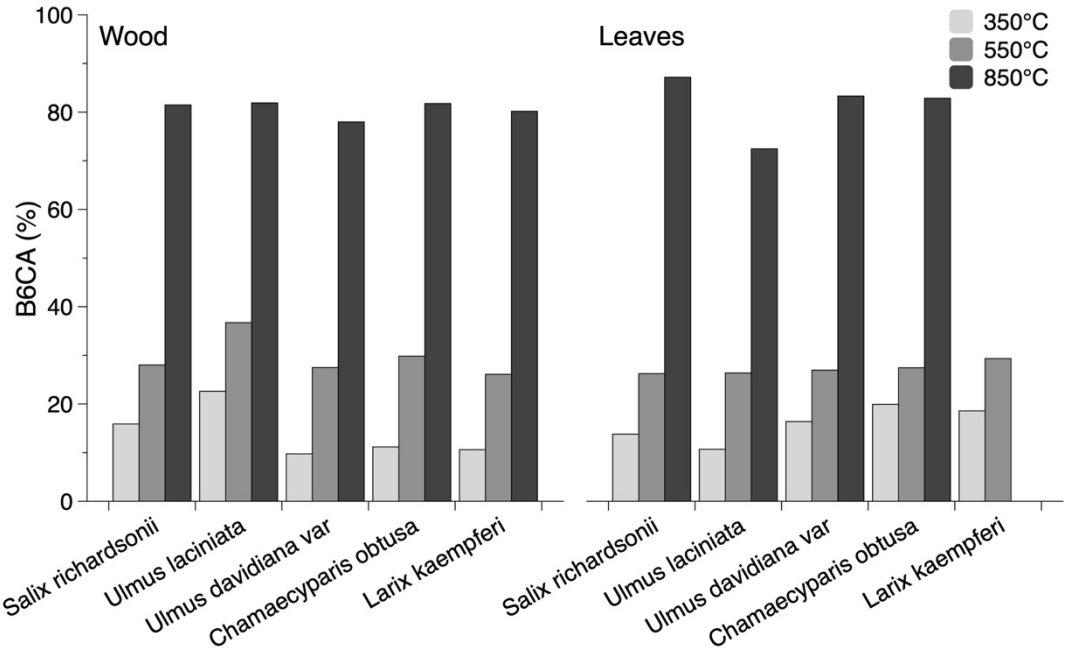

Figure 14. B6CA (%) in wood and leaves charcoal with pyrolysis temperature at 350 °C, 550 °C, and 850 °C. Treatment temperatures are shown as silver gray for 350 °C, tin gray for 550 °C , and tungsten gray for 850 °C.

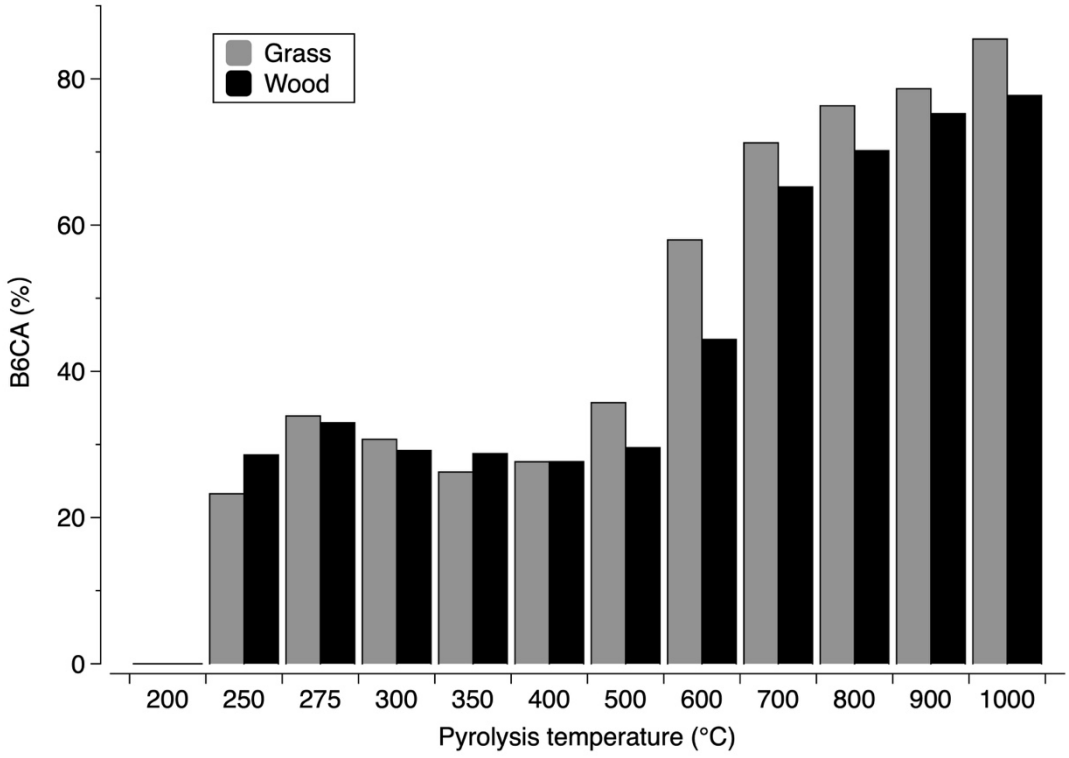

Figure 15. B6CA (%) in European grass and wood charcoal with pyrolysis temperature at 200 ~ 1000 °C. Treatment temperatures are shown as tin gray for grass , and tungsten gray for wood.

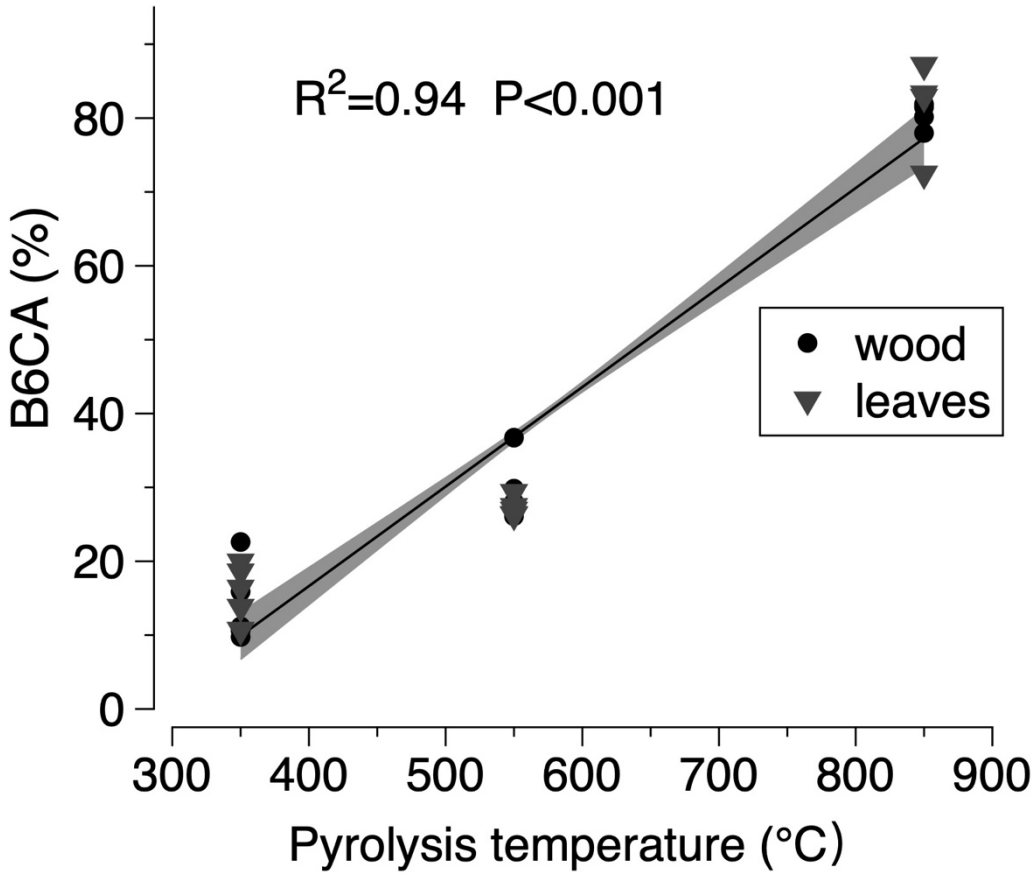

Figure 16. Relationship between B6CA (%) and pyrolysis temperature for the total samples. The grey lines represent the 95% of confidence interval envelopes. The wood and leaves charcoal (5 plants) are shown as black dots and gray inverted triangle, respectively.

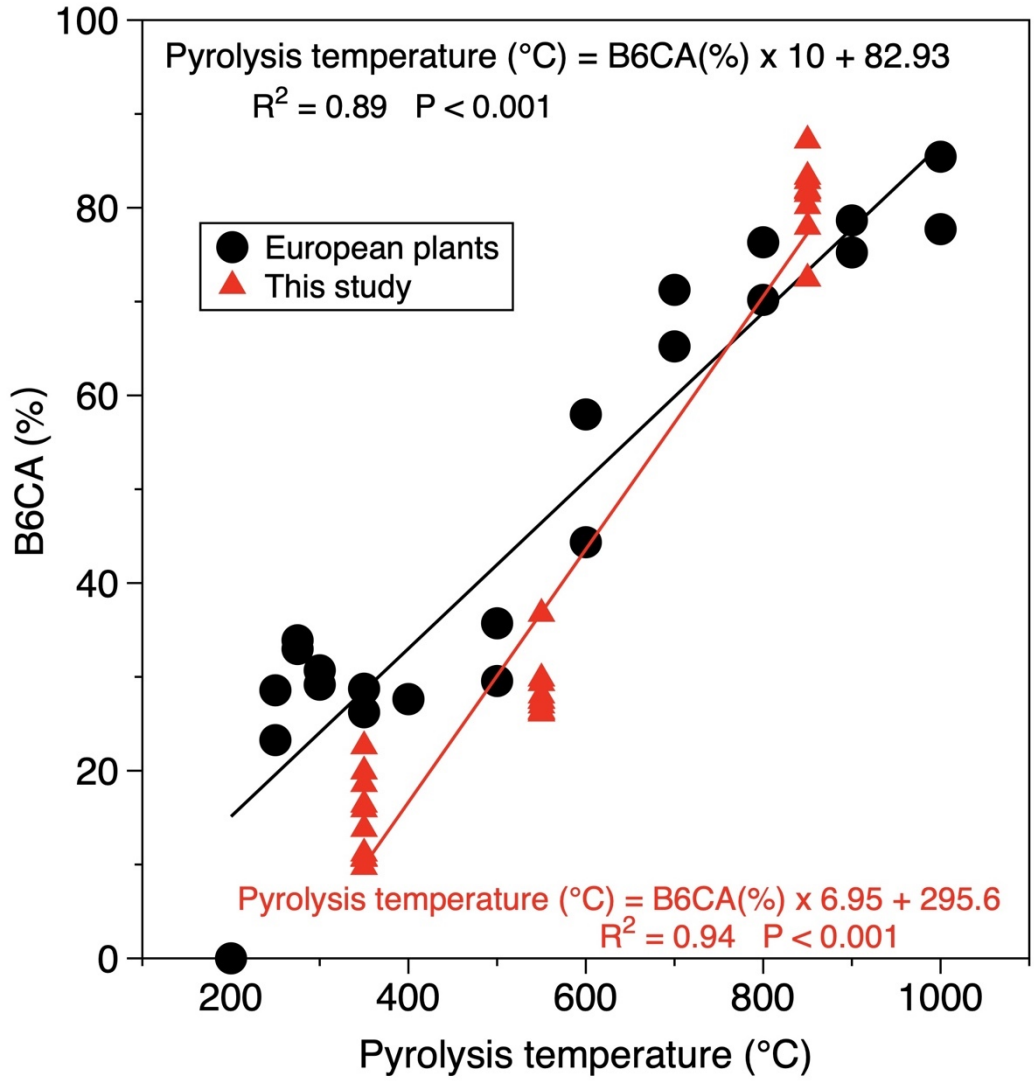

Figure 17. Relationship between B6CA (%) and pyrolysis temperature for the European and East Asian samples. The European plants and East Asian plants charcoal are shown as black dots and red inverted triangle, respectively.

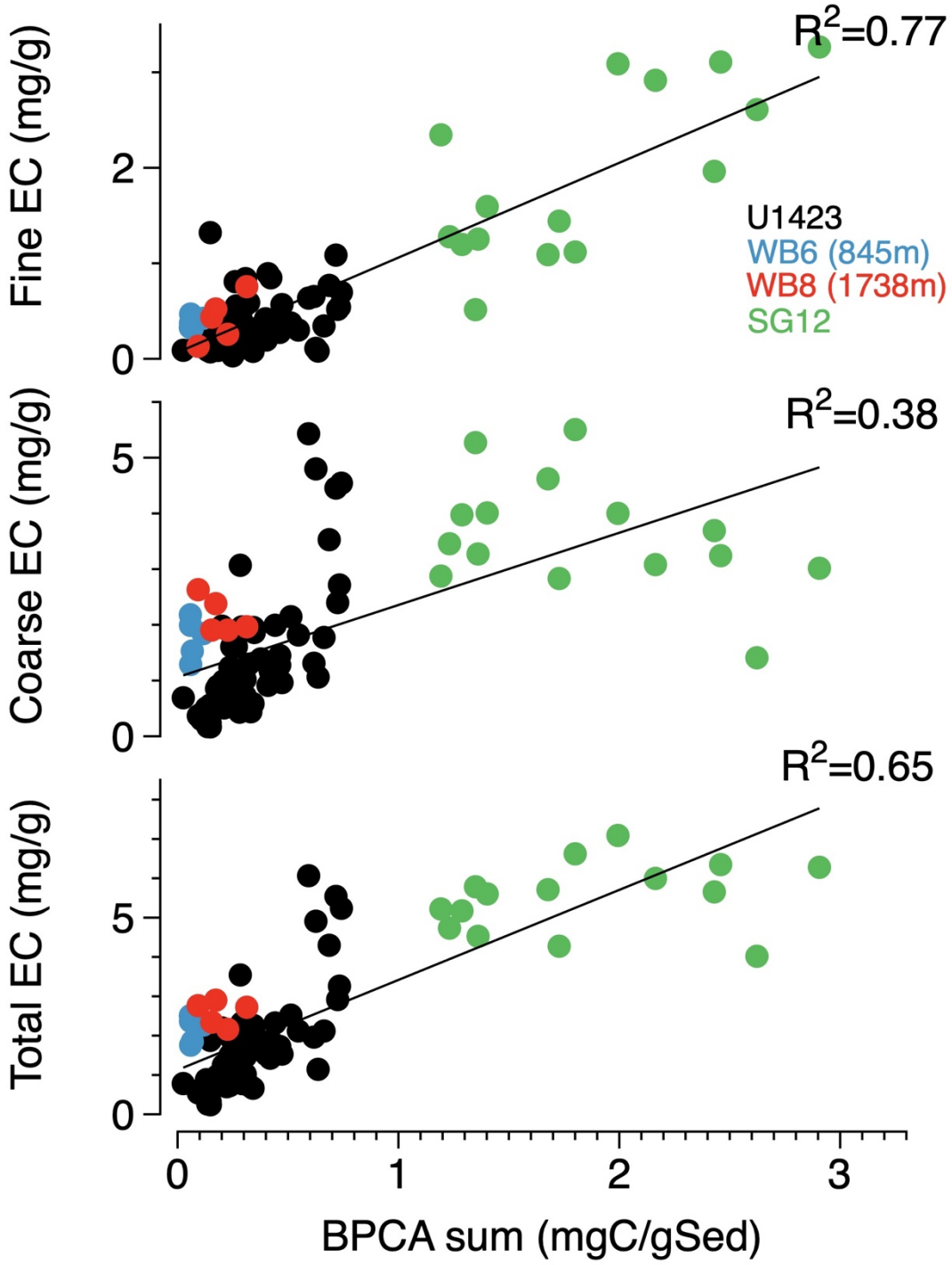

Figure 18. Relationship between BPCA sum and Total EC (include: Coarse EC, Fine EC) content for the total samples. The samples of Japan Sea U1423, Wakasa Bay KR15-10 Sites WB6 & 8 and Lake Suigetsu SG-12 are shown as black dots, blue dots, red dots and green dots, respectively.

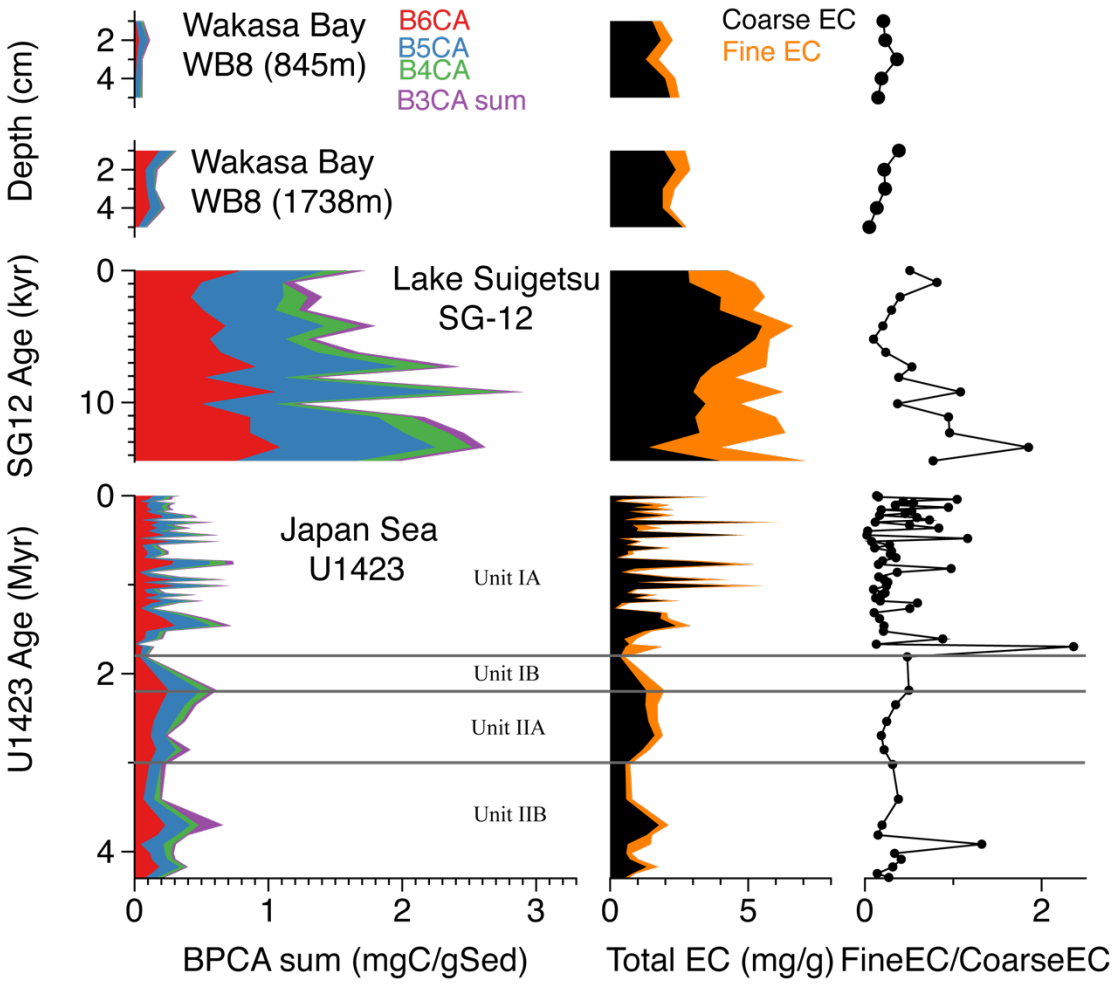

Figure 19. Temporal variations in contents of B6CA, B5CA, B4CA, B3CA, BPCA sum, coarse EC, fine EC, total EC and the ratio of Fine EC / Coarse EC. The contents of B6CA, B5CA, B4CA, B3CA, coarse EC, fine EC are represented as red, blue , green, pink, black, orange color. The ratio of Fine EC / Coarse EC are shown as black line.

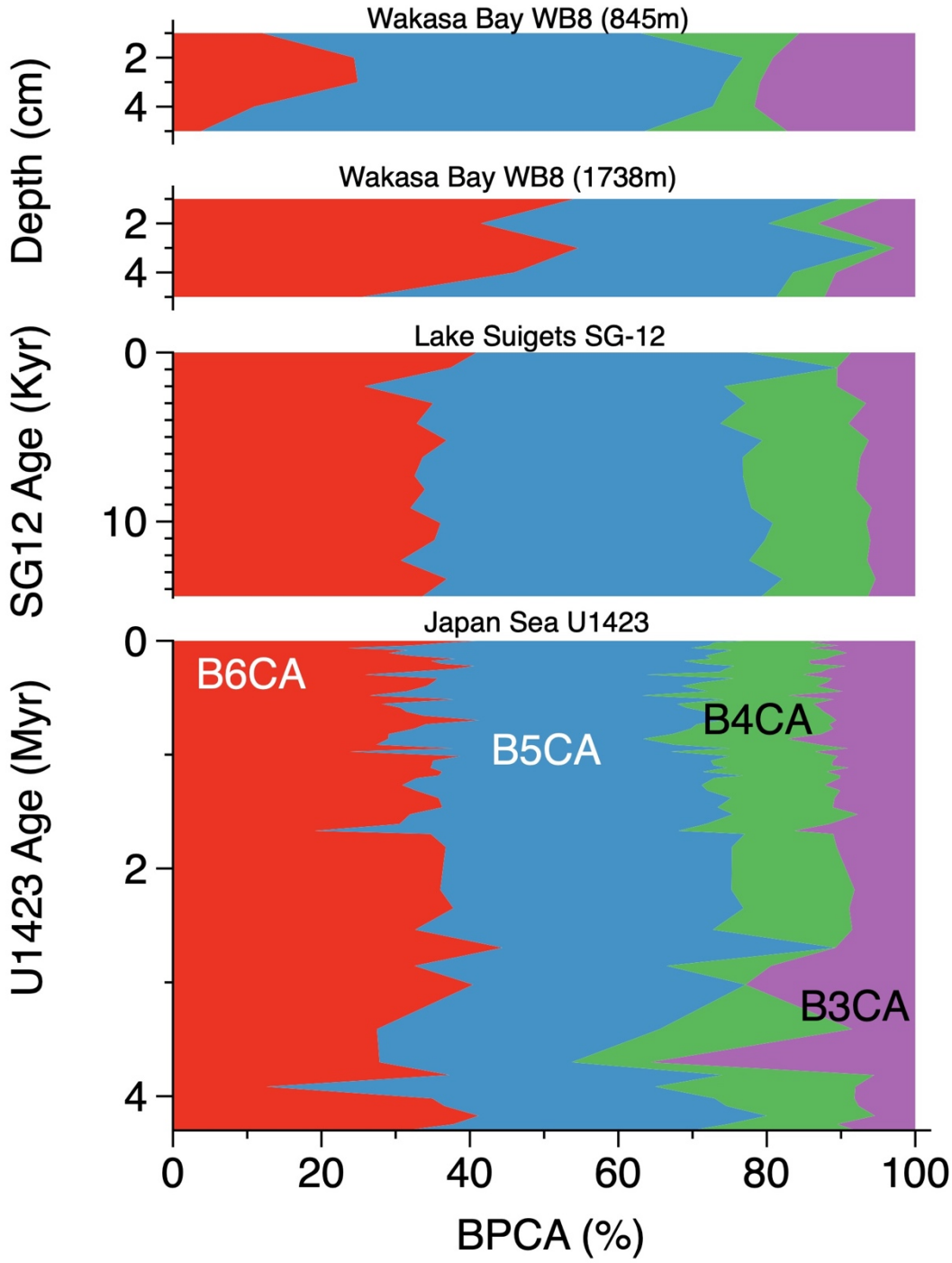

Figure 20. Temporal variations in B6CA (%), B5CA (%), B4CA (%) and B3CA (%). The B6CA (%), B5CA (%), B4CA (%) and B3CA (%) are represented as red, blue , green and pink color.

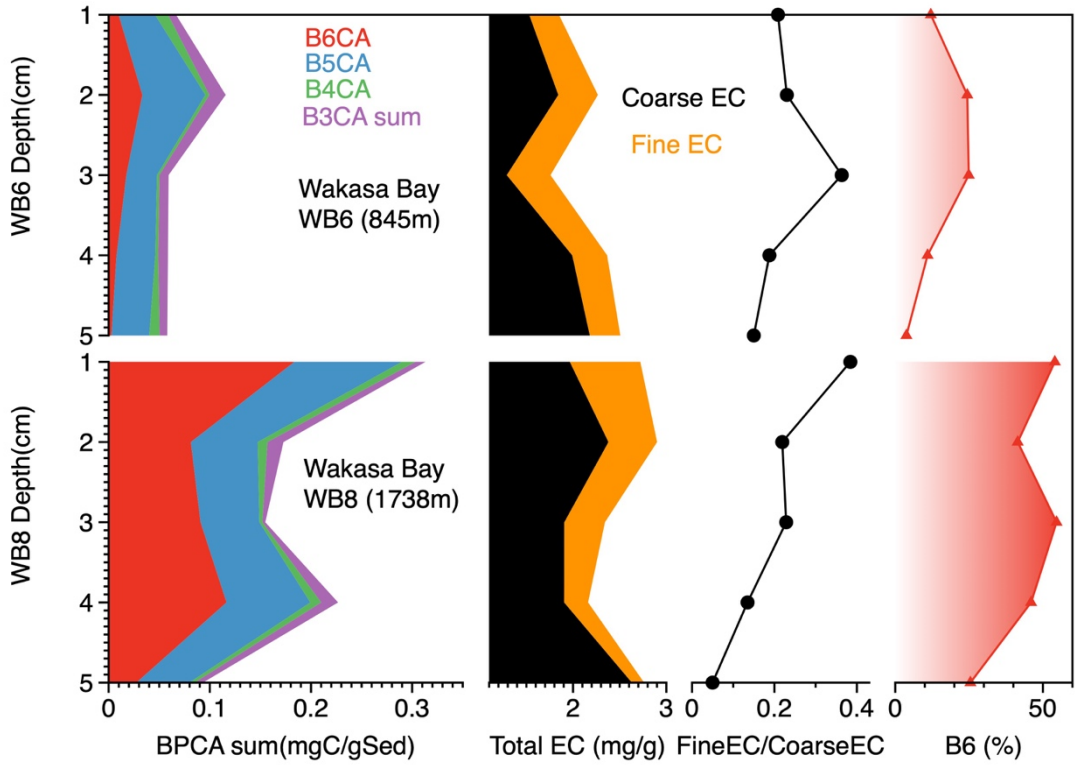

Figure 21. Temporal variations in contents of B6CA, B5CA, B4CA, B3CA, BPCA sum, coarse EC, fine EC, total EC, the ratio of Fine EC / Coarse EC and B6CA (%). The contents of B6CA, B5CA, B4CA, B3CA, coarse EC, fine EC are represented as red, blue , green, pink, black, orange color. The ratio of Fine EC / Coarse EC are shown as black line. B6CA (%) are represented as gradient red color.

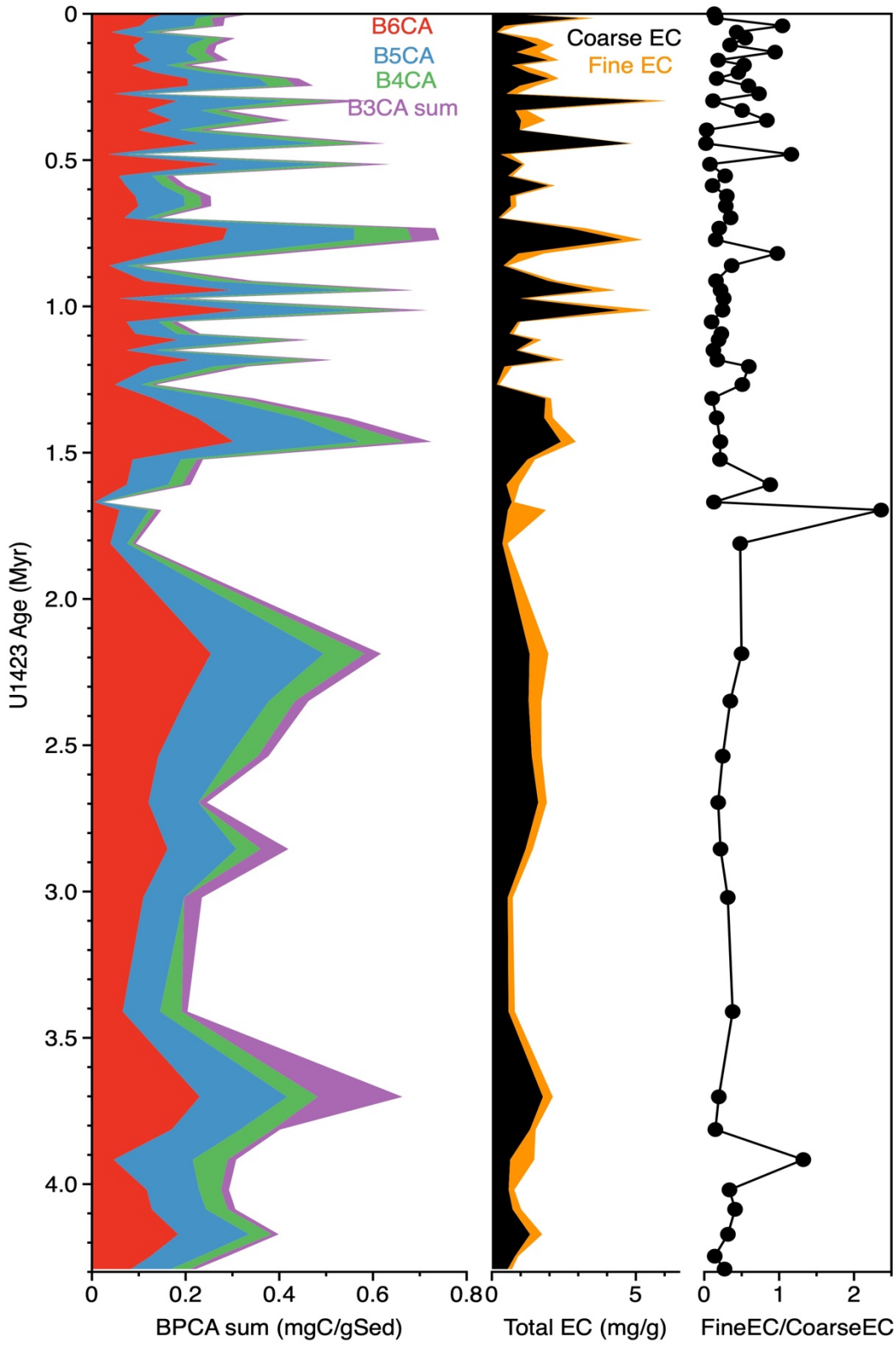

Figure 22. Temporal variations in contents of B6CA, B5CA, B4CA, B3CA, BPCA sum, coarse EC, fine EC, total EC and the ratio of Fine EC / Coarse EC. The contents of B6CA, B5CA, B4CA, B3CA, coarse EC, fine EC are represented as red, blue , green, pink, black, orange color. The ratio of Fine EC / Coarse EC are shown as black line.

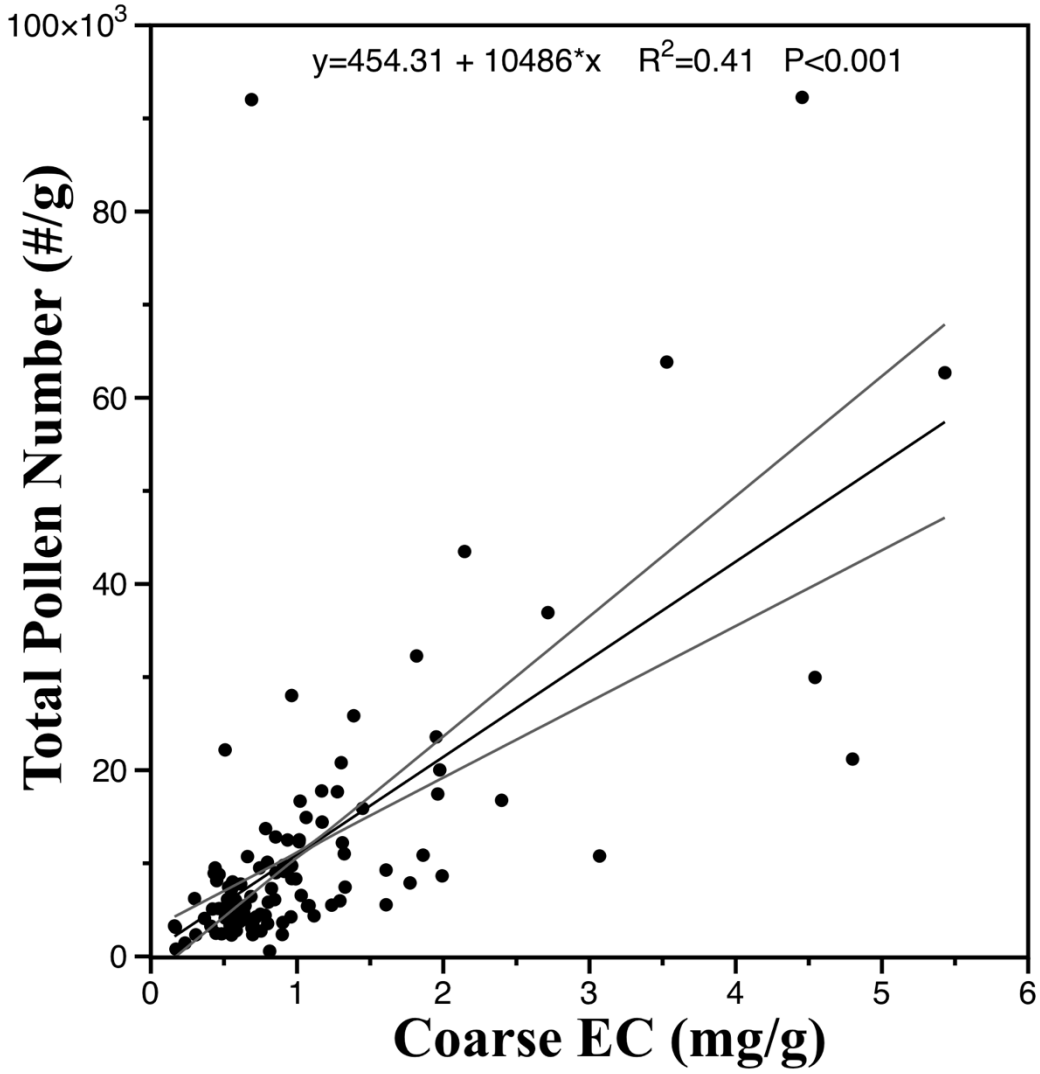

Figure 23. Relationship between pollen content and EC content in the coarse fraction at Site U1423. The grey lines represent the 95% of confidence interval envelopes.

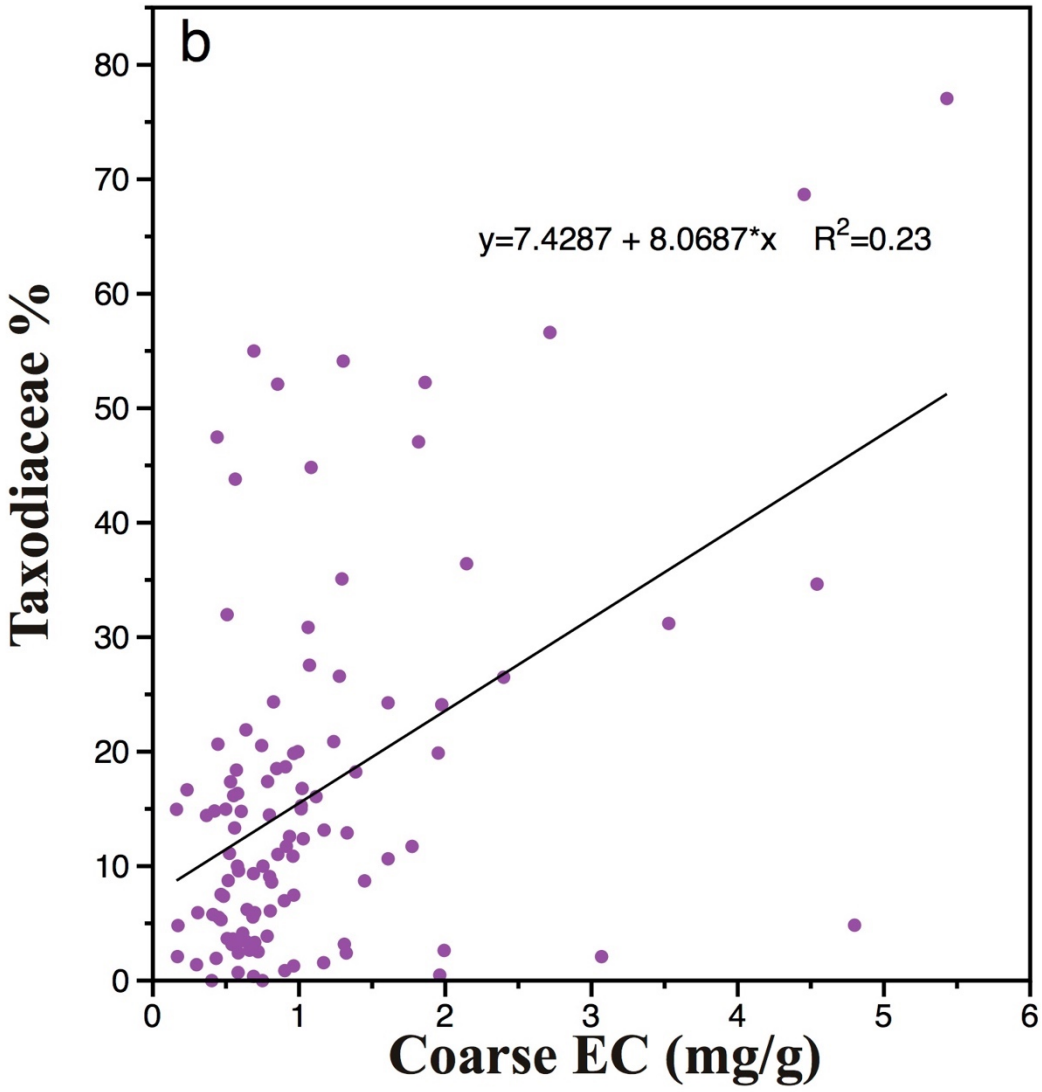

Figure 24. Relationship between Taxodiaceae and EC content in the coarse fraction at Site U1423.

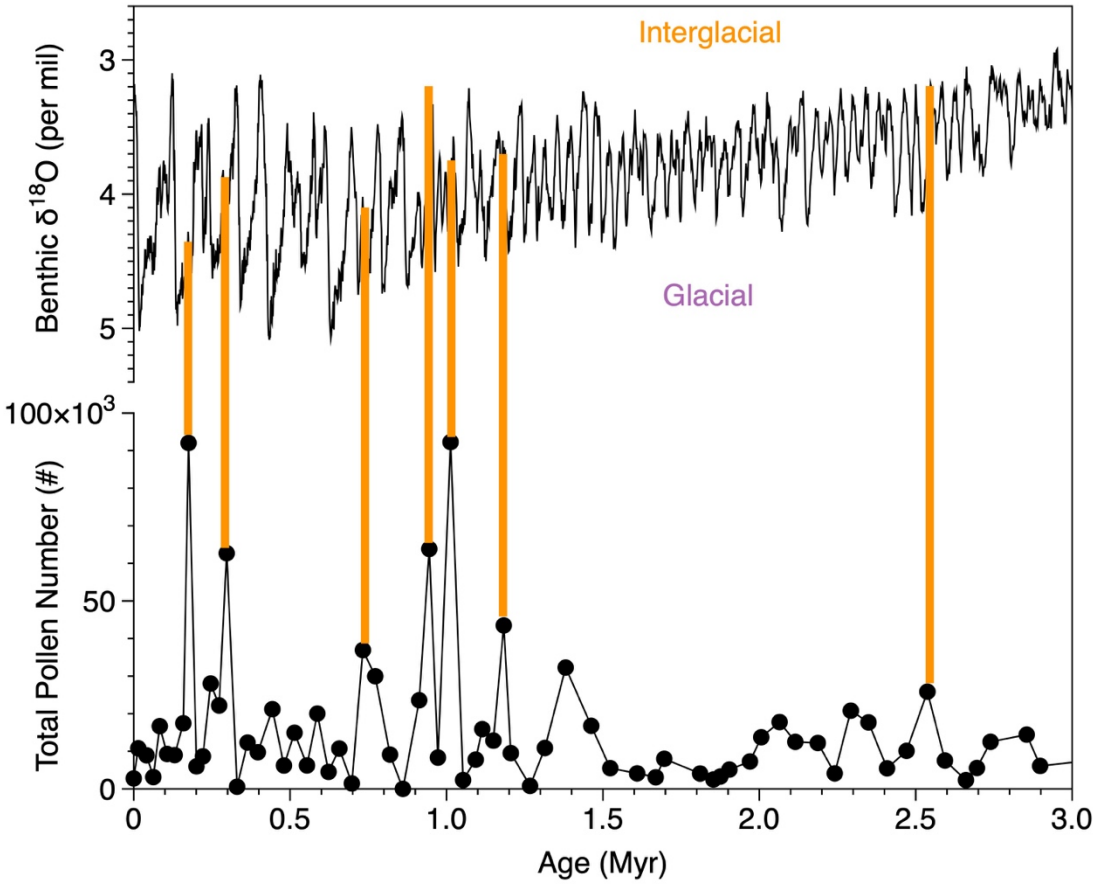

Figure 25. LR04 standard benthic δ18O (Lisiecki and Raymo, 2005) and pollen content. The significant maxima observed in the pollen content are marked as orange vertical lines corresponding to interglacial stages.

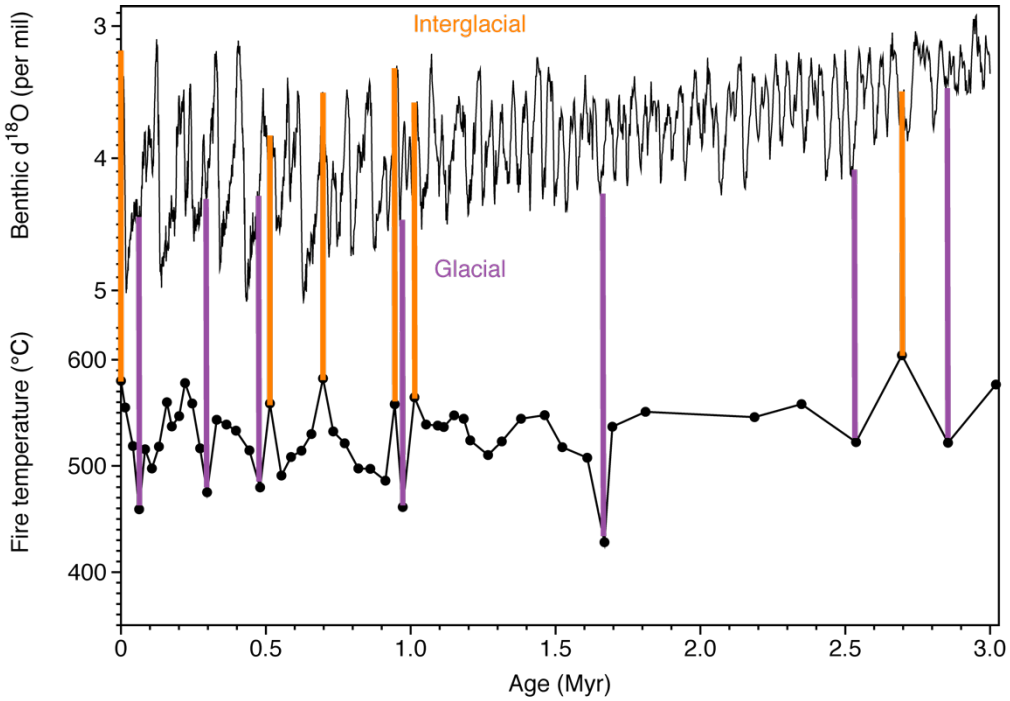

Figure 26. LR04 standard benthic δ18O (Lisiecki and Raymo, 2005) and the fire temperature estimated from B6CA (%). The significant observed in the low and higher temperature biomass burning are marked as pink and orange vertical lines corresponding to glacial and interglacial stages, respectively.

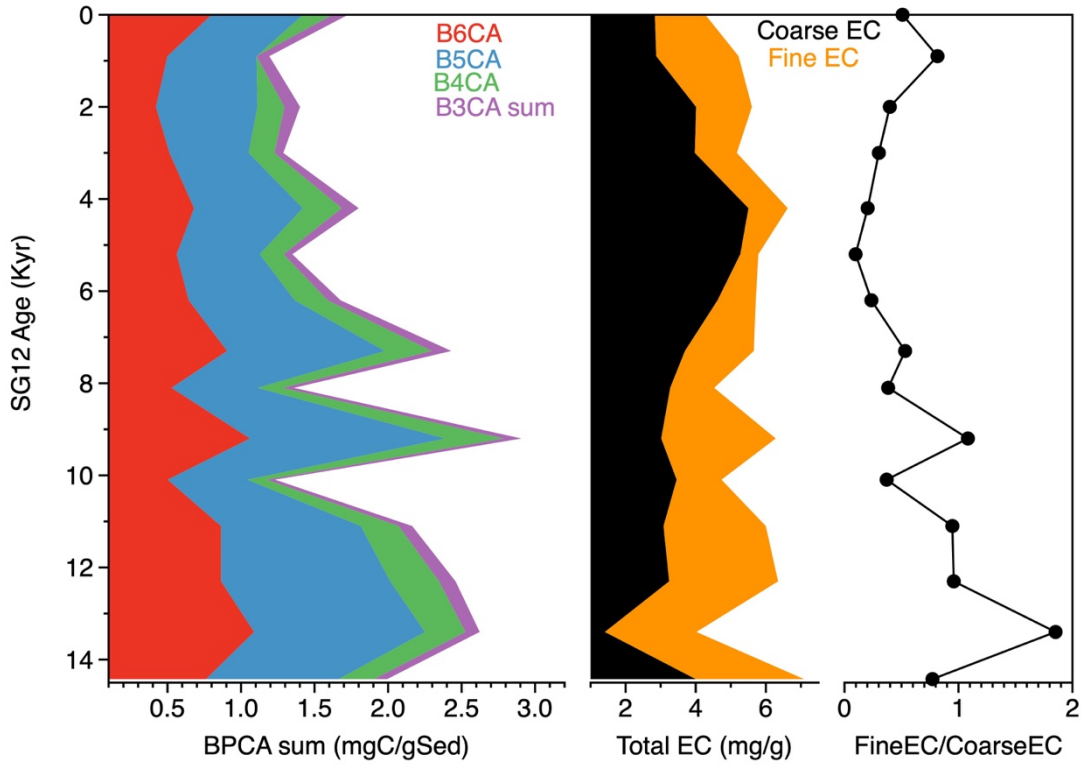

Figure 27. Temporal variations in contents of B6CA, B5CA, B4CA, B3CA, BPCA sum, coarse EC, fine EC, total EC and the ratio of Fine EC / Coarse EC. The contents of B6CA, B5CA, B4CA, B3CA, coarse EC, fine EC are represented as red, blue , green, pink, black, orange color. The ratio of Fine EC / Coarse EC are shown as black line.

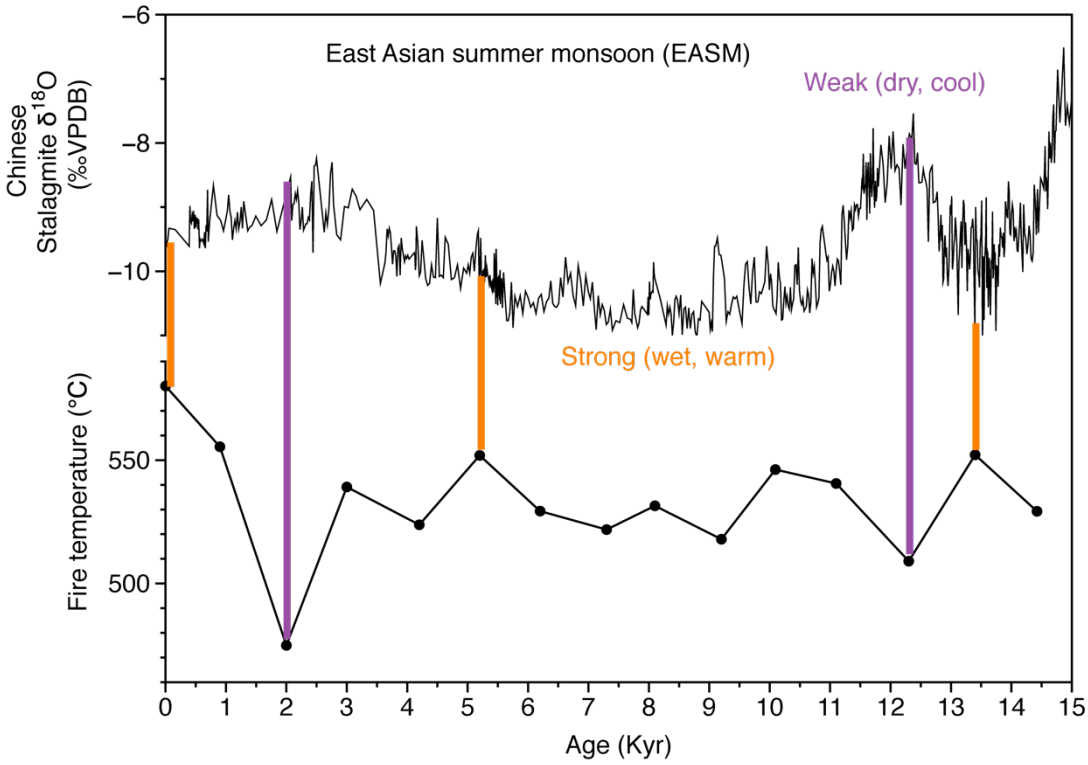

Figure 28. Chinese Stalagmite δ18O (Cheng et al., 2016) and the fire temperature estimated from B6CA (%). The significant observed in the low and higher temperature biomass burning are marked as pink and orange vertical lines corresponding to East Asian summer monsoon (EASM) weak and strong stages, respectively.

Table

Table 1. The plant species settings for this study.

Botanical name	Kind	Location	Fuel material		Pyrolysis temperature
Salix richardsonii ヤナギ	N/A	Siberia	Branch	Leaf	350℃, 550℃, 850℃
Ulmus laciniata オヒョウ	Broadleaf	North Japan	Branch	Leaf	350℃, 550℃, 850℃
Ulmus davidiana var アキニレ	Broadleaf	South Japan	Branch	Leaf	350℃, 550℃, 850℃
Chamaecyparis obtusa ヒノキ	Conifer	South Japan	Branch	Leaf	350℃, 550℃, 850℃
Larix kaempferi カラマツ	Conifer	North Japan	Branch	Leaf	350℃, 550℃, 850℃

Table 2. The control points for age model.

Type P: Projected from U1424 D: Direct turning to LR04

Exp	Site	Hole	Core	Type	Sect	A/W	Offset (cm)	CCSF-D_Patched_rev20150416 (m)	LR04 Age (Ma)	Type
346	U1423	B	1	H	2	A	1	1.45	0.02	P
346	U1423	A	1	H	2	A	148	2.86	0.03	P
346	U1423	A	1	H	3	A	72	3.60	0.04	P
346	U1423	A	1	H	3	A	136	4.22	0.05	P
346	U1423	A	1	H	4	A	40	4.76	0.06	P
346	U1423	B	2	H	3	A	4	7.43	0.09	P
346	U1423	B	2	H	4	A	74	9.63	0.11	P
346	U1423	B	2	H	6	A	49	12.38	0.14	P
346	U1423	A	2	H	4	A	130	13.43	0.15	P
346	U1423	A	2	H	5	A	123	14.91	0.17	P
346	U1423	A	2	H	6	A	62	15.80	0.18	P
346	U1423	B	3	H	2	A	108	16.89	0.20	P
346	U1423	B	3	H	3	A	138	18.69	0.22	P
346	U1423	B	3	H	4	A	54	19.35	0.23	P
346	U1423	B	3	H	4	A	118	19.99	0.24	P
346	U1423	B	3	H	5	A	120	21.51	0.26	P
346	U1423	B	3	H	6	A	137	23.18	0.29	P
346	U1423	A	3	H	5	A	126	24.83	0.32	P
346	U1423	B	4	H	3	A	2	27.16	0.36	P
346	U1423	B	4	H	4	A	60	29.24	0.41	P
346	U1423	B	4	H	6	A	53	32.17	0.47	P
346	U1423	B	4	H	6	A	93	32.57	0.48	P
346	U1423	A	4	H	5	A	16	33.82	0.50	P
346	U1423	A	4	H	6	A	107	36.22	0.55	P
346	U1423	B	5	H	2	A	150	36.90	0.56	P
346	U1423	B	5	H	3	A	96	37.86	0.58	P
346	U1423	B	5	H	5	A	1	39.95	0.61	P
346	U1423	B	5	H	5	A	85	40.79	0.63	P
346	U1423	A	5	H	4	A	123	43.57	0.68	P
346	U1423	A	5	H	5	A	66.5	44.50	0.70	P
346	U1423	A	5	H	6	A	68	46.02	0.73	P
346	U1423	B	6	H	3	A	2	47.16	0.74	P
346	U1423	B	6	H	4	A	3	48.67	0.76	P
346	U1423	B	6	H	4	A	58	49.22	0.77	P
346	U1423	B	6	H	5	A	18	50.32	0.80	P
346	U1423	B	6	H	5	A	133.5	51.47	0.82	P
346	U1423	A	6	H	4	A	133	53.37	0.85	P

346	U1423	A	6	H	5	A	45	53.96	0.87	P
346	U1423	A	6	H	5	A	130	54.81	0.88	P
346	U1423	A	6	H	6	A	24.5	55.26	0.89	P
346	U1423	A	6	H	6	A	105	56.06	0.91	P
346	U1423	B	7	H	3	A	16	56.74	0.93	P
346	U1423	B	7	H	4	A	63	58.71	0.97	P
346	U1423	B	7	H	4	A	131	59.39	0.98	P
346	U1423	B	7	H	5	A	54	60.12	0.99	P
346	U1423	B	7	H	5	A	87	60.45	1.00	P
346	U1423	B	7	H	5	A	139	60.97	1.00	P
346	U1423	B	7	H	6	A	120	62.28	1.01	P
346	U1423	A	7	H	4	A	79	62.96	1.01	P
346	U1423	B	8	H	1	A	109.5	64.82	1.08	P
346	U1423	A	7	H	5	A	144	65.43	1.09	P
346	U1423	B	8	H	2	A	135.5	66.44	1.11	P
346	U1423	B	8	H	3	A	44	67.02	1.13	P
346	U1423	B	8	H	3	A	123	67.81	1.14	P
346	U1423	B	8	H	5	A	149	71.07	1.18	P
346	U1423	A	8	H	3	A	98	72.07	1.19	P
346	U1423	A	8	H	4	A	70.5	73.30	1.23	P
346	U1423	A	8	H	4	A	138	73.97	1.26	P
346	U1423	B	9	H	1	A	132	75.16	1.29	P
346	U1423	A	8	H	6	A	31	76.04	1.31	P
346	U1423	B	9	H	2	A	140	76.64	1.34	P
346	U1423	B	9	H	4	A	14.5	78.38	1.41	P
346	U1423	B	9	H	4	A	53	78.77	1.42	P
346	U1423	B	9	H	4	A	137	79.61	1.46	P
346	U1423	B	1	H	1	A	137.5	1.31	0.01	D
346	U1423	A	1	H	3	A	14.7	3.03	0.03	D
346	U1423	A	1	H	4	A	47.5	4.84	0.06	D
346	U1423	A	1	H	5	A	20.6	6.07	0.07	D
346	U1423	B	2	H	2	A	114.4	7.04	0.08	D
346	U1423	B	2	H	3	A	11.2	7.51	0.09	D
346	U1423	B	2	H	3	A	116.2	8.56	0.10	D
346	U1423	B	2	H	4	A	105	9.94	0.11	D
346	U1423	B	2	H	5	A	75.9	11.15	0.12	D
346	U1423	B	2	H	5	A	135.9	11.75	0.13	D
346	U1423	A	2	H	6	A	106.3	16.24	0.19	D
346	U1423	B	3	H	7	A	4.2	23.35	0.30	D
346	U1423	A	3	H	6	A	48.6	25.55	0.34	D
346	U1423	B	4	H	3	A	67	27.81	0.37	D
346	U1423	B	4	H	5	A	31.7	30.45	0.42	D

346	U1423	A	4	H	6	A	68.1	35.83	0.53	D
346	U1423	B	5	H	3	A	49.8	37.40	0.56	D
346	U1423	B	5	H	3	A	96	37.86	0.58	D
346	U1423	B	5	H	5	A	76.2	40.70	0.62	D
346	U1423	A	5	H	4	A	92.5	43.26	0.68	D
346	U1423	A	5	H	5	A	134.9	45.19	0.71	D
346	U1423	B	6	H	4	A	5	48.69	0.76	D
346	U1423	B	6	H	4	A	140	50.04	0.79	D
346	U1423	B	6	H	5	A	106.5	51.20	0.81	D
346	U1423	A	6	H	4	A	133	53.37	0.85	D
346	U1423	A	6	H	5	A	47.3	53.98	0.87	D
346	U1423	A	6	H	6	A	64.2	55.65	0.90	D
346	U1423	A	6	H	7	A	5	56.37	0.92	D
346	U1423	B	7	H	3	A	66.3	57.24	0.94	D
346	U1423	B	7	H	4	A	27.5	58.35	0.96	D
346	U1423	B	7	H	4	A	77.5	58.85	0.97	D
346	U1423	B	7	H	4	A	127.5	59.35	0.98	D
346	U1423	A	7	H	4	A	65	62.82	1.01	D
346	U1423	A	7	H	4	A	127.5	63.45	1.03	D
346	U1423	B	8	H	1	A	65	64.38	1.06	D
346	U1423	A	7	H	5	A	102.2	65.02	1.08	D
346	U1423	B	8	H	2	A	131.5	66.40	1.10	D
346	U1423	B	8	H	3	A	31.9	66.90	1.11	D
346	U1423	B	8	H	3	A	141.9	68.00	1.14	D
346	U1423	B	8	H	6	A	85	71.93	1.19	D
346	U1423	A	8	H	4	A	17.5	72.77	1.22	D
346	U1423	A	8	H	4	A	102.5	73.62	1.24	D
346	U1423	A	8	H	4	A	138	73.97	1.26	D
346	U1423	B	9	H	1	A	42.5	74.27	1.26	D
346	U1423	B	9	H	1	A	125	75.09	1.29	D
346	U1423	B	9	H	2	A	42	75.76	1.30	D
346	U1423	A	8	H	6	A	50.3	76.23	1.32	D
346	U1423	B	9	H	3	A	6	76.80	1.34	D
346	U1423	B	9	H	3	A	51	77.25	1.36	D
346	U1423	B	9	H	3	A	106	77.80	1.38	D
346	U1423	B	9	H	4	A	12.5	78.36	1.41	D
346	U1423	B	9	H	4	A	67.5	78.91	1.42	D
346	U1423	B	9	H	4	A	130	79.54	1.45	D
346	U1423	B	9	H	4	A	145	79.69	1.46	D
346	U1423	B	9	H	5	A	19	79.93	1.46	D
346	U1423	B	9	H	5	A	89	80.63	1.48	D
346	U1423	B	9	H	5	A	124	80.98	1.48	D

346	U1423	B	9	H	5	A	141.5	81.15	1.49	D
346	U1423	B	9	H	6	A	20.3	81.44	1.50	D
346	U1423	B	9	H	6	A	42.8	81.67	1.52	D
346	U1423	B	9	H	6	A	75.3	81.99	1.54	D
346	U1423	B	9	H	6	A	117.8	82.42	1.55	D
346	U1423	B	9	H	6	A	145.3	82.69	1.56	D
346	U1423	B	9	H	7	A	11.7	82.86	1.57	D
346	U1423	A	9	H	4	A	77.5	83.24	1.58	D
346	U1423	A	9	H	4	A	102.5	83.49	1.59	D
346	U1423	A	9	H	4	A	137.5	83.84	1.59	D
346	U1423	A	9	H	4	A	140	83.86	1.60	D
346	U1423	A	9	H	5	A	11.7	84.08	1.62	D
346	U1423	A	9	H	5	A	54.2	84.51	1.63	D
346	U1423	A	9	H	5	A	71.7	84.68	1.63	D
346	U1423	A	9	H	5	A	101.7	84.98	1.66	D
346	U1423	B	10	H	2	A	90.4	86.40	1.68	D
346	U1423	B	10	H	2	A	127.9	86.77	1.68	D
346	U1423	B	10	H	3	A	26.8	87.26	1.68	D
346	U1423	B	10	H	3	A	69.3	87.69	1.71	D
346	U1423	B	10	H	3	A	106.8	88.06	1.72	D
346	U1423	B	10	H	3	A	121.8	88.21	1.73	D
346	U1423	B	10	H	4	A	7.5	88.57	1.75	D
346	U1423	B	10	H	4	A	27.5	88.77	1.77	D
346	U1423	B	10	H	4	A	47.5	88.97	1.80	D
346	U1423	B	10	H	4	A	92.5	89.42	1.81	D
346	U1423	B	10	H	5	A	28.9	90.28	1.82	D
346	U1423	B	10	H	5	A	78.9	90.78	1.83	D
346	U1423	B	10	H	5	A	123.9	91.23	1.85	D
346	U1423	B	10	H	6	A	8	91.57	1.86	D
346	U1423	B	10	H	6	A	43	91.92	1.86	D
346	U1423	A	10	H	4	A	140	93.77	1.89	D
346	U1423	A	10	H	5	A	104.3	94.91	1.91	D
346	U1423	A	10	H	6	A	7.9	95.45	1.93	D
346	U1423	A	10	H	6	A	72.9	96.10	1.95	D
346	U1423	B	11	H	2	A	144.6	97.21	1.98	D
346	U1423	B	11	H	3	A	10.5	97.37	1.99	D
346	U1423	B	11	H	3	A	128	98.54	2.01	D
346	U1423	B	11	H	4	A	72.5	99.49	2.01	D
346	U1423	B	11	H	4	A	107.5	99.84	2.05	D
346	U1423	B	11	H	4	A	147.5	100.24	2.06	D
346	U1423	B	11	H	5	A	91.7	101.18	2.07	D
346	U1423	B	11	H	6	A	15	101.91	2.10	D

346	U1423	B	11	H	6	A	55	102.31	2.11	D
346	U1423	A	11	H	4	A	70	102.87	2.12	D
346	U1423	A	11	H	4	A	112.5	103.30	2.14	D
346	U1423	A	11	H	5	A	21.6	103.89	2.16	D
346	U1423	A	11	H	5	A	71.6	104.39	2.18	D
346	U1423	A	11	H	6	A	3.4	105.21	2.20	D
346	U1423	A	11	H	6	A	55.9	105.73	2.21	D
346	U1423	A	11	H	6	A	140.9	106.58	2.24	D
346	U1423	B	12	H	2	A	142.2	107.15	2.26	D
346	U1423	B	12	H	3	A	111.3	108.34	2.28	D
346	U1423	B	12	H	4	A	20	108.92	2.30	D
346	U1423	A	12	H	2	A	68.3	109.52	2.32	D
346	U1423	B	12	H	4	A	142.5	110.24	2.34	D
346	U1423	B	12	H	5	A	104	111.36	2.36	D
346	U1423	B	12	H	6	A	37.5	112.19	2.38	D
346	U1423	A	12	H	5	A	69.3	113.48	2.43	D
346	U1423	A	12	H	6	A	19	114.48	2.46	D
346	U1423	A	12	H	6	A	114	115.43	2.49	D
346	U1423	A	12	H	6	A	144	115.73	2.50	D
346	U1423	A	12	H	7	A	10.9	115.89	2.52	D
346	U1423	B	13	H	2	A	72.7	116.50	2.55	D
346	U1423	B	13	H	3	A	42.1	117.70	2.57	D
346	U1423	B	13	H	3	A	74.6	118.02	2.59	D
346	U1423	B	13	H	3	A	119.6	118.47	2.60	D
346	U1423	B	13	H	4	A	82.5	119.60	2.65	D
346	U1423	B	13	H	5	A	8.9	120.37	2.66	D
346	U1423	A	13	H	4	A	2.5	121.71	2.69	D
346	U1423	A	13	H	4	A	90	122.58	2.70	D
346	U1423	B	13	H	6	A	127.9	123.23	2.72	D
346	U1423	A	13	H	5	A	112	124.22	2.74	D
346	U1423	A	13	H	5	A	147	124.57	2.78	D
346	U1423	B	14	H	1	A	95	125.23	2.81	D
346	U1423	B	14	H	2	A	0	125.78	2.83	D
346	U1423	B	14	H	2	A	25	126.03	2.85	D
346	U1423	B	14	H	3	A	4.5	127.32	2.89	D
346	U1423	B	14	H	3	A	99.5	128.27	2.90	D
346	U1423	B	14	H	3	A	134.5	128.62	2.92	D
346	U1423	B	14	H	4	A	5	128.83	2.95	D
346	U1423	B	14	H	4	A	45	129.23	2.98	D
346	U1423	B	14	H	4	A	80	129.58	2.99	D